Universality in selection with local perturbations in the Saffman-Taylor problem

Bruce E. Shaw
Department of Physics and The James Franck Institute, University of Chicago, 5640 South Ellis Avenue, Chicago, Illinois 60637
(Received 28 November 1988)

An analytic theory using WKBJ methods for selection with local perturbations in the Saffman-Taylor [Proc. R. Soc. London, Ser. A **245**, 312 (1958)] problem is presented. I obtain qualitative agreement with previously published phenomenology, including symmetric narrowed fingers for local reductions in the surface-tension parameter, narrowed asymmetric fingers for local increases, and scaling of the tip curvature and asymmetry with the square root of the surface-tension parameter. The source of the universality in the perturbed problem is discussed, giving some explanation of why the experimental perturbations can be modeled by locally varying surface tension. Very good quantitative agreement between theory and a numerical simulation of the same perturbation is shown, with no adjustable parameters to fit. Finally, I outline experiments to test new behavior predicted by the theory; a quantitative prediction observable experimentally is given.

I. INTRODUCTION

Recently, much attention has been given to moving free-boundary problems, both because of their relevance to interesting physical systems, and because of some of the surprising and elegant answers that have been found to long-standing puzzles. The growth of dendritic solids from liquid melt,[1] electrodeposition,[2–4] and diffusion-limited aggregation[5] (DLA) are a few such systems. The shape of the boundary between two different phases—liquid-gas, nematic-isotropic, occupied-unoccupied—is studied as one phase is driven to grow at the expense of another. We search for similarity solutions in time, for example, translation at constant velocity, or scale invariance, and then examine how these states can be reached, and their stability. The problem of fingering in two-dimensional viscous fluid flow has connections to a number of different topics arising in the free-boundary studies. In what follows in the introduction, I will set up the problem to be considered here, and point out some of these connections.

A. Equation and boundary conditions

The physical system consists of two closely spaced glass plates, called a Hele-Shaw cell,[6] filled with two immiscible fluids. The boundary between them is studied when one fluid is pushed against the other. The laminar viscous flow allows averaging over the small plate separation, so we can consider just a two-dimensional problem. In the viscous fluid there is no inertial term, so the velocity of the fluids moves with the gradient of the pressure: $\mathbf{v}\sim\nabla p$. Taken with the incompressibility of the fluid, $\nabla\cdot\mathbf{v}=0$ we get the pressure field satisfied Laplace's equation $\nabla^2 p=0$.

At the walls of the channel, and at infinity, we have fixed boundary conditions: there is no flow through the walls, and a uniform flow down the channel at infinity. The difficulty is the free interface boundary. The interface moves with the local fluid velocity, given a dynamical boundary condition that $\mathbf{v}_i\cdot\hat{\mathbf{n}}=\text{const}\times\nabla p\cdot\hat{\mathbf{n}}$, where v_i is the interface velocity and $\hat{\mathbf{n}}$ is the unit normal to to interface. The other interface condition in the fingering problem is a static one. When the viscosity of the pushing fluid is much smaller, we can take the pressure as being constant throughout it. Then the static boundary condition is $p=TK$, where T is the surface tension and K is the curvature.

There are many closely related physical problems with this same dynamic boundary condition, but a different differential equation or static boundary condition. Generalizing Laplace's equation to the diffusion equation gives a whole class of problems called Stefan problems: dendritic growth and directional solidification are two examples with the same free-boundary conditions as the case of viscous fingering.[7] The equation for fingering in a non-Newtonian fluid involves an extra term in the differential equation; there, a highly ramified branching pattern, like DLA, is seen.[8] In DLA, there is a noise term added to the dynamic condition, while the surface tension is zero. If we mimic the boundary conditions of the fluids, using DLA walkers, by reducing the noise and adding surface tension, fingering like that of the fluids is observed.[9] In this paper I generalize the static boundary condition to allow for local variations in the surface tension.

B. Selection problem

In the absence of surface tension, continuous families of exact solutions are known in the fingering[10] and dendrite problems.[11] Experimentally, however, it is found that a unique solution is selected for each value of the surface tension parameter. This situation has arisen in a number of systems: when we neglect in a simplified model a physical effect that seems to be small, we get a continuum of solutions, but including this term selects a particular solution. These kinds of perturbations are called singular perturbations. Current research on directional solidification,[12] viscous fingering, and dendrites[13] is studying questions of selection and singular perturbations. In this paper, I will develop the theory for the

variation in the selected solution when the static boundary condition is changed locally.

Thirty years ago Saffman and Taylor found a two-parameter family of finger solutions in a channel at zero surface tension: one parameter represented the width of the finger, and the other the asymmetry in the channel.[14] But when the experiment was done, only one solution was observed, the symmetric finger whose width went to $\frac{1}{2}$ from above as the surface tension went to zero.[15] The question that remained unresolved until recently was why this particular solution was selected. McLean and Saffman, when they put surface tension into the problem, obtained an integrodifferential equation which they solved numerically, and found a selected width for nonzero surface tension.[16] But at the same time, in carrying out a regular perturbation expansion in the surface tension, to all orders no selection mechanism was found. The problem was finally tackled analytically in the last few years.[17–21] The techniques involved taking the exact solution for zero surface tension, and then looking at the correction to the shape of the finger due to surface tension. The surface-tension term is proportional to the curvature, and in the equations this term is a singular perturbation. It turned out that the solutions to these equations contained terms exponentially small in the surface tension which were causing the selection. This is why no selection was seen in the regular perturbation expansion.

Next, it was found that local perturbations to the interface could drastically alter the selected finger solution. When small bubbles were placed at the tip of a finger, narrowed fingers with widths well below the $\frac{1}{2}$ barrier were obtained by Couder *et al.*[22] In experiments with thin wires, narrowed asymmetric fingers were observed. A numerical simulation in which the surface tension was locally varied also gave narrowed asymmetric fingers for local increases, and symmetric solutions for local decreases; similar scaling laws for the asymmetry and tip curvature as a function of the dimensionless surface-tension parameter were seen in the experiment and simulation of Zocchi, Shaw, Libchaber, and Kadanoff (ZSLK).[23,24] An alternative model for the effect of the bubble has been given by Hong and Langer[25] who considered the bubble as giving a finite positive cusp at the tip of the finger. Hong has also modeled the wire by a negative cusp.[26] Later I will comment on the relation of their model to the technique used here.

It is the purpose of this paper to explain this more general selection problem when there are perturbations present. I obtain qualitative agreement with the phenomenology of the perturbed problem, scaling laws consistent with observed values, and very good direct quantitative comparison between theory and simulation. Additionally, features of the theory which ought to be observable experimentally are discussed, and measurements which would test these predictions presented.

C. Outline of the paper

In the absence of surface tension, the interface is a line of constant pressure. Surface tension adds a correction that changes the condition for the field on the boundary. The pressure is now a constant times the curvature—a nonlinear function of the shape. The method I will use was developed by Tanveer.[27] The method consists of transforming this boundary condition into a differential equation for the correction to the exact solution, and taking advantage of the small surface-tension parameter on the highest derivative to use WKBJ techniques.[28] Following ZSLK, I will generalize the method to allow for variable surface tension, with perturbations represented by local variations.

The calculation proceeds as follows. In Sec. II I analytically continue and linearize a real equation that must be satisfied on the interface. This gives a complex linear ordinary differential equation for the correction to the shape of the finger due to surface tension. The technique is Tanveer's, my only modification being the generalization of allowing for spatially dependent surface tension. At the end Sec. II I discuss the form of the surface-tension perturbations to be used. We then have a complete formulation of the problem. In Secs. III and IV I solve the equations. The idea is to find solutions good at each tail, and continue them forward to the tip, where they should match. For general finger width and asymmetry we will find the solutions good at each tail do not match at the tip. In Sec. III I follow how Tanveer calculates the mismatch of the solutions in the case of constant surface tension, presenting it in a way that can be used for the generalized nonconstant surface-tension problem. The new work is contained in Sec. IV. There I calculate the contributions to the matching of the solutions at the tip due to local variations in surface tension. An explicit expression for one localized perturbation is given, as well as a general equation for multiple perturbations. Section V discusses the results of the calculation. I get symmetry relations for the different perturbations, scaling relations, quantitative comparison between theory and simulation, and predictions for experiments. The reader not interested in the details of the calculation can skip to Sec. V; I summarize there the equations that I will use that were derived in the first three sections.

II. FORMULATION OF THE PROBLEM

In this section I outline the method of Tanveer, while modifying it to allow for varying surface tension. We begin with the boundary condition at the interface for a "steady-state" finger moving at constant velocity down the channel. We analytically continue this condition on the shape of the finger, and get a second-order ordinary differential equation for the correction to the shape of the finger due to surface tension. Along the way we linearize the differential equation, while keeping the highest derivative which is a singular perturbation to the ODE. In the last part of this section I discuss the form of the perturbations used in this paper. Later on in the paper, I will discuss how the differential equation is solved.

A. Setting up the calculation

1. Boundary conditions for the shape correction

The pressure field ϕ satisfies Laplace's equation, so we can write it as the real part of an analytic velocity poten-

tial $W(z)=\phi+i\psi$. This is an analytic function of the spatial variable $z=x+iy$, where x is the distance down the channel and y is the direction across. Change to a reference frame moving at velocity U so that the finger is at rest. The statement that it is a steady state is that the finger boundary is a streamline;

$$\psi=0 \tag{1}$$

on the finger boundary. In the moving frame ϕ is just ϕ_{rest} in the rest frame minus the translated velocity times x: $\phi+Ux=\phi_{\text{rest}}$. The surface tension on the boundary gives ϕ_{rest}, and we get

$$\phi+Ux=\frac{b^2T}{w^2 12\mu}\tau K+\text{const} . \tag{2}$$

Here K is the curvature of the boundary. The constant coefficient $b^2T/w^2 12\mu$ comes from the Hele-Shaw cell approximation: b is the plate separation, w the channel width, μ the fluid viscosity, and T the surface tension. The thing that is new is τ. The function τ will be allowed to vary in space; it represents a perturbation to the interface. It is the point of this paper to show how the introduction of a τ which is nonconstant alters the selection mechanism.

We are going to be doing many analytic continuations. Rather than work in physical z space, it is more convenient to map conformally the fluid region onto a simpler domain. We map the fluid to the upper half unit disc in the ζ plane, with the finger boundary corresponding to the unit semicircle, and the walls being mapped to the real diameter. The solution is the function which maps this domain back to the physical plane, while respecting the boundary conditions there. We write the solution as

$$\begin{aligned} z=&\frac{2}{\pi}f(\zeta)-\frac{2}{\pi}\ln\zeta+\frac{2}{\pi}(1-\lambda)(1-\cos\beta)\ln(\zeta-1)\\ &+\frac{2}{\pi}(1-\lambda)(1+\cos\beta)\ln(\zeta+1)\\ &-i2(1-\lambda)(1-\cos\beta)+i . \end{aligned} \tag{3}$$

The right-hand side, except for f, is the exact two-parameter family of solutions for zero surface tension found by Saffman and Taylor. The fraction of the width of the channel filled by the finger is λ, while

$$a=(1-\lambda)\cos\beta \tag{4}$$

is the asymmetry of the finger, and is the displacement of the finger from the center of the channel ($a=0$ is a symmetric finger). The correction to the shape of the finger due to surface tension is f.

To represent the effect of no flow through the walls we map the fluid onto the upper half plane, and set

$$\text{Im}f=0 \tag{5}$$

on the real diameter. (The real axis is like a "mirror"). Our other condition for f comes from Eqs. (1)–(3). Combining them, choosing the appropriate origin for z, and properly analytically continuing, we get

$$\text{Re}f=-G\tau(\zeta)K(\zeta) . \tag{6}$$

G is a dimensionless surface tension

$$G=\frac{b^2\pi^2T}{12w^2\mu U} . \tag{7}$$

The curvature K can be written as

$$K(\zeta)=\frac{1}{|f'+h|}\left[1+\text{Re}\left[\zeta\frac{d}{d\zeta}\ln(f'+h)\right]\right] , \tag{8}$$

where $f'+h=(\pi/2)dz/d\zeta$. Our plan is to analytically continue this equation for f, in order to write it as a differential equation. When later on we do this continuation we will need the analytic structure of h, defined by its zeros and poles:

$$h(\zeta)=\frac{(1-p_1\zeta)(1+p_2\zeta)}{\zeta(\zeta^2-1)} , \tag{9}$$

where

$$p_1=a+[a^2+(2\lambda-1)]^{1/2} \tag{10}$$

and

$$p_2=-a+[a^2+(2\lambda-1)]^{1/2} . \tag{11}$$

Equation (6) is a nonlinear differential equation for f. The equation can be linearized by taking $|f'/h|\ll 1$. Tanveer solves the uniform surface-tension problem for both the nonlinear equation and the linearized equation. He finds the same qualitative behavior, with slight quantitative differences. Because I expect the features again to be essentially given by the linearized problem, and since the linear analysis is much simpler and can be treated further analytically, I will take only that approach in this paper.

2. *Linearization and analytic continuation*

To linear (6) we take f'/h to be small. This approximation will work except at the zeros of h. At the zeros of h the dominant term is f'/h^2, so we keep this term in the linearization, which is now valid everywhere. The result is

$$\frac{1}{\tau}|h|\,\text{Re}(f)+G\,\text{Re}\left[\zeta\left[\frac{f'}{h}\right]'\right]+G\,\text{Re}\left[1+\zeta\frac{h'}{h}\right]=0 . \tag{12}$$

When we finish the calculation, we will have to go back to see that the terms that were dropped were done consistently. Rather than waiting for the end of the calculation to justify the linearization, I will note now the order of the terms: away from the singularities of h, $f/G\sim G^{-1/2}$, $f'\sim 1$, $f''\sim G^{-1/2}$; near the zero $-1/p_2$ of h, $f'/h\sim 1$ and the contributions come from a neighborhood $<G^{-1/2}$, so that Gf'/h^2 does indeed dominate the ff'/h term neglected in the linearization.

The next step is to analytically continue this real equation (12), valid on the unit circle, to a complex equation valid everywhere. While the details are interesting, I will

only sketch them here, since Tanveer goes through them carefully, and the only modification is to replace $|h|$ by $|h|/\tau$. Define a new analytic function g with the property that

$$\mathrm{Re}g = \frac{1}{\tau}|h|\,\mathrm{Re}f \tag{13}$$

on the unit circle. Then (12) becomes

$$\mathrm{Re}\left[\frac{G\zeta}{h}f'' - \frac{G\zeta h'}{h^2}f' + G\left[1+\zeta\frac{h'}{h}\right]+g\right]=0\ . \tag{14}$$

Being careful about the kinds of singularities in (14), Tanveer shows that the analytic continuation of (14) is just the expression inside the brackets, which vanishes everywhere. Now to find g. Using the Poisson integral formula to find g inside the unit circle from its real part on the unit circle, and using $\zeta^* = 1/\zeta$ on the unit circle, gives g in terms of an integral on the unit circle of a kernel times $f(\zeta)+f(1/\zeta)$. The next step is to continue this expression to find g outside the unit circle. This involves deforming the contour outside the circle, and gives some extra residues from the singularities of the kernel. The net result is to get an expression for g which is given by an integral over the unit circle plus an algebraic function times $f(\zeta)+f(1/\zeta)$. We now have an expression involving $f''(\zeta)$, $f'(\zeta)$, $f(\zeta)$, $f(1/\zeta)$, and an integral of $f(\zeta)+f(1/\zeta)$.

The continuation uses the symmetry imposed by the walls, that $|h(\zeta)|\,\mathrm{Re}f(\zeta)=|h(\zeta^*)|\mathrm{Re}f(\zeta^*)$ on the unit circle. This symmetry will also have to be present in τ: $\tau(\zeta)=\tau(\zeta^*)$ on $|\zeta|=1$. Taken with the condition that τ is real on the unit circle, this gives

$$\mathrm{Im}[\tau]=0 \tag{15}$$

on the real diameter.

The final step giving the differential equation is to restrict the region of validity to having ζ be on or outside the unit circle. This is done to simplify the term we have involving $f(1/\zeta)$, and the integral of $f(\zeta)+f(1/\zeta)$ on the unit circle. Then our equation will only involve $f(\zeta)$ and its derivatives. For ζ on or in the unit circle, if we write f as a regular perturbation expansion,

$$f=\sum_{n=1}^{\infty} G^n f_n\ , \tag{16}$$

the corrections to this expansion will be exponentially small. For ζ outside the unit circle, the corrections can become large. It is for this reason we will be examining the equation in that domain, where these otherwise hidden transcendentally small terms can become large enough to be seen. If we restrict the region of validity of the equation to be for $|\zeta|\geq 1$ then we can replace $f(1/\zeta)$ by the first term in the regular perturbation expansion, $f_1(1/\zeta)$, where

$$f_1(\zeta)=\frac{1}{4\pi i}\oint_{|\zeta'|=1}\frac{d\zeta'}{\zeta}\left[\frac{\zeta+\zeta'}{\zeta'-\zeta}+\frac{1+\zeta\zeta'}{1-\zeta\zeta'}\right] \times\frac{1+\mathrm{Re}(\zeta+\zeta h/h')}{|h|}\tau(\zeta')\ , \tag{17}$$

which is valid for $|\zeta|<1$.

The result is that the continued equation is now

$$f''+Qf'+\frac{L}{\tau G}f=R\ , \tag{18}$$

with

$$Q=-\frac{h'}{h}\ , \tag{19}$$

$$L=\frac{h|h|}{\zeta} =i\frac{(\zeta-p_1)^{1/2}(\zeta+p_2)^{1/2}(1+\zeta p_2)^{3/2}(1-\zeta p_1)^{3/2}}{\zeta^2(\zeta^2-1)^2}\ , \tag{20}$$

$$R=-h'-\frac{h}{\zeta}-\frac{I_2(f_1,\zeta)h}{\zeta}-\frac{L}{\tau}f_1(1/\zeta)\ . \tag{21}$$

The term I_2 is the analytic continuation of $|h|\,\mathrm{Re}f_1$, but it will not play any role in the rest of the calculation. This is a linear second order differential equation for the shape correction f. Solving it correctly will be a long and difficult task. To complete the specification of the problem, we need the function τ. In the next section I discuss this function τ, which represents perturbations to the finger interface.

B. Form of τ

I now present the form of the perturbations I will use in this paper. Here, the idea of universality is very important. The experiments with a wire, and simulations which used localized surface-tension perturbations which were Gaussian functions of the lateral direction y, showed very similar behavior (ZSLK). There was no physical connection between the form of the perturbation in the simulation and the wire, other than that both were localized. It is then hoped that this lack dependence on the specific form of the perturbation will also show up in the analytic treatment. Thus, rather than trying to recreate a very complex physical system of a wetting wire intersecting a moving meniscus, I seek a form simple analytically, out of which more complicated forms could be built if desired. Later, we will be able to see the source of this universality.

Physically, we want something localized in space. Mathematically, the effect of the function is seen through its zeros and poles. The simplest structure is a ratio of polynomials. Let us work this out in the ζ plane, building in the proper symmetries. The lowest order would be a dipole

$$\frac{\zeta-\zeta_0 r_t}{\zeta-\zeta_0 r_s}\ , \tag{22}$$

where ζ_0 is some point on the unit semicircle and r_t and r_s are positive real numbers (since we do not want any zeros or poles on the finger, they should also not equal 1). We have to preserve the symmetries that $\mathrm{Im}\tau=0$ on the real diameter and on the unit circle. That means $\tau(\zeta)=\tau(1/\zeta)=\tau^*(\zeta)$. Building that all in gives

$$\frac{1}{\tau(\zeta)}=\frac{(\zeta-\zeta_0 r_t)(\zeta-\zeta_0/r_t)}{(\zeta-\zeta_0 r_s)(\zeta-\zeta_0/r_s)}\frac{(\zeta\zeta_0-r_t)(\zeta\zeta_0-1/r_t)}{(\zeta\zeta_0-r_s)(\zeta\zeta_0-1/r_s)} . \tag{23}$$

This expression has the form of two quadrupoles, one in the upper half plane, and one reflected about the real axis in the lower. To get a feel for what this τ perturbation looks like, let us write it in another form. For $\zeta_0=e^{i\nu_0}$, and

$$r_t+\frac{1}{r_t}=2+\sigma^2 , \tag{24}$$

$$r_s+\frac{1}{r_s}=2+\sigma^2(1+A) \tag{25}$$

on the unit circle (23) can be rewritten as

$$\tau=\left[1+\frac{A}{1+[2-2\cos(\nu-\nu_0)]/\sigma^2}\right]\times\left[1+\frac{A}{1+[2-2\cos(\nu+\nu_0)]/\sigma^2}\right] . \tag{26}$$

For small σ this is a function which is nearly constant away from ν_0, and varies locally at ν_0 with a range σ and amplitude A. For $\nu\neq\nu_0$ and σ very small, the denominators will be very large, and τ will be essentially 1. At $\nu=\nu_0$, $\tau=1+A$. The definitions (24) and (25) for r_s and r_t gave a simple expression for (26). When working with the representation of τ given by (23), however, it is simpler to define r_s and r_t by

$$r_t=1+\sigma , \tag{27}$$

$$r_s=1+\sigma\sqrt{1+A} . \tag{28}$$

This is the definition of r_s and r_t I will use in the paper. This gives basically the same perturbation as (26): a quadratically falling even perturbation in ν with width σ and amplitude A, with

$$-1<A<\infty , \tag{29}$$

$$\sigma>0 . \tag{30}$$

Finally, I can build up nearly any perturbation by composing these elemental τ's:

$$\tau=\prod_{n=0}^{n_{\max}}\tau_n(\nu_n,A_n,\sigma_n) . \tag{31}$$

We will see later, however, that for small perturbations many of the results are quite independent of the details of the perturbation, and they can be characterized in a most simple universal way.

III. MISMATCH IN THE CONSTANT-τ PROBLEM

We now proceed to solve the differential equation (18), taking advantage of the smallness of the parameter G. We construct a particular solution analytic everywhere along the finger boundary, with no exponentially growing parts. We will see this can only be done for special values of the width and asymmetry, and this will be the selection condition. In this section I show how Tanveer obtains the mismatch of the solutions good at each tail. The new work is contained in Sec. IV, where I calculate the contributions for quadrupole perturbations, giving the general selection for multiple quadrupoles and the explicit expression for a single quadrupole.

A. WKBJ solutions and matched asymptotic expansions

In the limit as $G\to 0$ there are two linearly independent WKBJ solutions to the homogeneous equation (18):

$$g_\alpha=h^{1/2}L^{-1/4}\tau^{1/4}e^{PG^{-1/2}} , \tag{32}$$

$$g_\beta=h^{1/2}L^{-1/4}\tau^{1/4}e^{-PG^{-1/2}} , \tag{33}$$

where

$$P(\zeta)=\int_{-1/p_2}^{\zeta}d\zeta' iL^{1/2}\tau^{-1/2} . \tag{34}$$

These solutions will be valid except where the approximation breaks down, at the zeros and poles of L and τ. The subtlety in these WKBJ problems is that the two true solutions, call them F_α and F_β, may be asymptotic to one linear combination of the WKBJ solutions in one sector of the plane, and to a different one in another sector.

A simple way to see the differing asymptotic combinations is to consider the function $2\cosh(\zeta^2G^{-1/2})$. For the argument of ζ: $-\pi/4<\arg(\zeta)<\pi/4$ and also on the similar wedge surrounding the negative real axis, this is asymptotic to $e^{\zeta^2G^{-1/2}}$, whereas in the two wedges between these two sectors it is asymptotic to $e^{-\zeta^2G^{-1/2}}$. The changeover occurs on the lines between the real and imaginary axes, where the terms are of comparable order, and one changes from being exponentially larger than the other to exponentially smaller. This illustrates a general feature, called the Stokes phenomenon: When passing through a line emanating from a turning point or pole on which the real part of P is constant (called a Stokes line), you can have the true solution be asymptotic to different linear combinations of the WKBJ solutions. (In the example mentioned above, $P=\zeta^2$ and the turning point is at $\zeta=0$.) We calculate these linear combinations by looking very close to those singularities. Then using the properties of the special functions which solve the locally simple differential equations, we can calculate the linear combination, or connection formula. This feature, that there can be exponentially small terms in the solution in one part of the plane which become exponentially large in another part of the plane, is what makes a naive regular perturbation treatment not work. The selection will come from making sure there are no exponentially growing parts.

A simple analogy to the calculation we will be doing is the one-dimensional quantum-mechanics oscillator problem. There, we start at $-\infty$ with the exponentially decaying solution, and continue it forward to the classical turning point. We "scatter" through the turning point, matching to the two oscillating solutions on the other side, then continue across to the second turning point. There we again scatter into the two solutions, one decay-

ing and the other growing exponentially. However, we want our solution to match to only the decaying solution. Only special isolated parameters will satisfy this condition, and these give the eigenvalues of the problem. We have a similar problem here: we want the shape correction to be have no exponentially growing parts on the finger. We can start at one tail of the finger, and continue around the tip, scattering when we pass through any turning points or poles. When we get around to the other tail, we want there to be none of the exponentially growing term mixed in. Another way is to start at both tails with the proper algebraic shape, and then continue forward to the tip on each side, demanding that they meet exactly with no discontinuities (that it is analytic). This matching near the tip is, in fact, what we do. It can be seen now, in a rough way, the effect of the perturbations: by adding turning points and poles to scatter the solutions good at the tails, they can change this "resonance" eigenvalue matching condition at the tip.

The plan is as follows. We first construct solutions good at each tail. These solutions will be made up of combinations of the homogeneous WKBJ solutions; more precisely, combinations of functions which are asymptotic to the WKBJ solutions. Then we learn how to continue the functions and solutions into other sectors where the original asymptotic expansions are no longer valid. When we have continued these solutions good at each tail to the tip, we will calculate how much they miss by. There will be a contribution to the mismatch due to the shape of the finger, and a contribution due to the local variations in the surface tension. Balancing the two contributions so there is no net mismatch will give the selection condition.

B. Solutions good at each tail

The method of variation of parameters gives us a particular solution to the inhomogeneous equation (18):

$$f = F_\beta(\zeta) \int_{\zeta_\alpha}^{\zeta} \frac{F_\alpha R}{W} d\zeta' - F_\alpha(\zeta) \int_{\zeta_\beta}^{\zeta} \frac{F_\beta R}{W} d\zeta' , \qquad (35)$$

where F_α and F_β are exact solutions to the homogeneous problem and ζ_α and ζ_β are constants. To this we can add any homogeneous solution; this is equivalent to changing the lower limits of integration. What does this solution look like? First, let us get a feel for the homogeneous solution. Asymptotically, they will be given by linear combinations of the two WKBJ solutions g_α and g_β. For $\mathrm{Re}P > 0$, g_α is exponentially large and g_β is exponentially small, and vice versa for $\mathrm{Re}P < 0$.

We are interested in both the constant ReP and ImP lines coming out of the singularities of τ and L. The constant ImP (anti-Stokes) lines are steepest descent paths, and across the constant ReP (Stokes) lines the exact homogeneous solutions F_α and F_β can be asymptotic to different linear combinations of the WKBJ solutions. For the case of $\lambda < \frac{1}{2}$ and the asymmetry parameter not too large, so that p_1 and p_2 are complex, the relevant lines of constant ReP and ImP are shown in Fig. 1 (see Tanveer, Fig. 10). In a later section, I will show what the Stokes lines for τ look like. The arrows point in the direction of increase (the opposite convention of Tanveer).

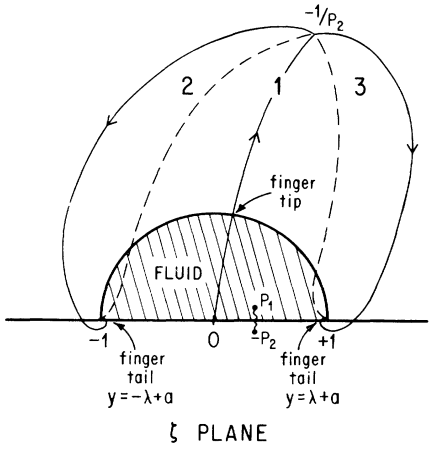

FIG. 1. Relevant Stokes (constant ReP, dashed lines) and anti-Stokes (constant ImP, solid lines) lines from $-1/p_2$ in the case of complex p_1 and p_2. The arrows are in the direction of increasing value. The numbers correspond to the sectors in the text.

We see that g_α becomes exponentially large in sectors 2 and 3 while g_β is in sector 1 (see Fig. 1). Fix the linear combinations by taking $F_\alpha \sim g_\alpha$ and $F_\beta \sim g_\beta$ in sector 2; this fixes their linear combination in all the other sectors as well, though it may be different in different ones. Now we want f to be an algebraic function; thus the coefficients multiplying the exponentially larger terms must be exponentially small. As this has to be valid at the tail $\zeta = -1$, this fixes one of the lower limits of integration in (35): $\zeta_\alpha = -1$. It turns out this linear combination is also valid into sector 1 (more about this later). By a similar argument, Re$P(\zeta_\beta)$ has to be at least as small as the smallest value of ReP on the unit circle. It turns out to be most convenient to choose $\zeta_\beta = 0$ as the lower limit, though this particular choice of ζ_β will drop out in the end and not affect anything (for a more detailed discussion of all this see Tanveer, pp. 1595 and 1596). This solution,

$$f = F_\beta(\zeta) \int_{0}^{\zeta} \frac{F_\alpha R}{W} d\zeta' - F_\alpha(\zeta) \int_{-1}^{\zeta} \frac{F_\beta R}{W} d\zeta' , \qquad (36)$$

works in sectors 2 and 1. Similarly, we can construct another solution,

$$\tilde{f} = \tilde{F}_\beta(\zeta) \int_{0}^{\zeta} \frac{\tilde{F}_\alpha R}{W} d\zeta' - \tilde{F}_\alpha(\zeta) \int_{1}^{\zeta} \frac{\tilde{F}_\beta R}{W} d\zeta' , \qquad (37)$$

valid in sectors 3 and 1, where $\tilde{F}_\beta \sim g_\beta$ and $\tilde{F}_\alpha \sim g_\alpha$ in sector 3. What we need to show is that we can match smoothly at the tip two solutions good at each tail. Our project, then, is to learn how to continue these solutions into other sectors to see if they match. It will turn out this matching can only be done for special discrete pairs of values for the finger width and asymmetry, and these depend on τ.

C. Shape mismatch M_S of f and $\tilde{f}$

To match f and $\tilde{f}$, we have to see how the F's continue. Let us first look at the constant-τ case. As I will show later, it turns out that $F_\alpha \sim g_\alpha$ in all the sectors. F_β, however, changes; for $F_\beta \sim g_\beta$ in sectors 2 and 1, we find $F_\beta \sim g_\beta + b_m g_\alpha \sim \tilde{F}_\beta + b_m F_\alpha$ in sector 3, where b_m is a constant I will give later. Let us try to match the f's.

I will write f in terms of $\tilde{f}$ plus some correction. To get the $\tilde{f}$ part, we need to change the lower limit of integration in the integral that is multiplying F_α: $\int_{-1}^{\xi} d\xi' F_\beta R/W \to \int_{1}^{\xi} d\xi' \tilde{F}_\beta R/W$. Note that we also had to change F_β to $\tilde{F}_\beta$. Since F_α blows up at $\xi=1$, we would not want to carry the $b_m F_\alpha$ piece out to there. Instead, we leave it behind along the way in the line integral, at the point p_m (more about p_m later). The paths of integration I will use here, which are discussed later on, are shown in Fig. 2.

One comment about notation: we are going to be seeing a lot of these $\int_{\xi_\alpha}^{\xi} d\xi' FR/W$ terms. To clean things up I will often drop the $d\xi' R/W$ and just symbolically write $\int_{\xi_\alpha}^{\xi} F$. That said, here goes;

$$
\begin{aligned}
f &= F_\beta \int_0^\xi d\xi' F_\alpha \frac{R}{W} - F_\alpha \int_{-1}^{\xi} d\xi' F_\beta \frac{R}{W} \\
&= (\tilde{F}_\beta + b_m F_\alpha) \int_0^\xi F_\alpha - F_\alpha \left[\int_{-1}^{p_m} F_\beta + \int_{p_m}^{\xi} b_m F_\alpha + \int_{p_m}^{1} \tilde{F}_\beta + \int_1^\xi \tilde{F}_\beta \right] \\
&= \tilde{F}_\beta \int_0^\xi F_\alpha - F_\alpha \int_1^\xi \tilde{F}_\beta + F_\alpha \left[\int_0^{p_m} b_m F_\alpha - \int_{-1}^{p_m} F_\beta - \int_{p_m}^{1} \tilde{F}_\beta \right] ,
\end{aligned} \tag{38}
$$

so

$$f = \tilde{f} + M_S F_\alpha , \tag{39}$$

where

$$M_S = b_m \int_0^{p_m} d\xi' F_\alpha \frac{R}{W} - \int_{-1}^{p_m} d\xi' F_\beta \frac{R}{W} - \int_{p_m}^{1} d\xi' \tilde{F}_\beta \frac{R}{W} . \tag{40}$$

Thus we see the difference between f and $\tilde{f}$ is a constant times F_α. The constant M_S depends on the shape of the finger; in the next section, I will evaluate this constant. Since F_α blows up on both sides, we cannot add or subtract any bit of it to f or $\tilde{f}$. Thus they cannot match.

This mismatch $M_S F_\alpha$ is the cusp that Hong and Langer[25] and Hong[26] consider. Note that it is a spatially dependent complex number, as F_α varies. The quantity $M_S F_\alpha$ turns out to be a positive real number at the tip. Moving along the interface it is complex, but becomes real and negative a distance $\sim G^{1/2}$ from the tip [see Sec. V A 3)]. That is the negative cusp Hong uses.

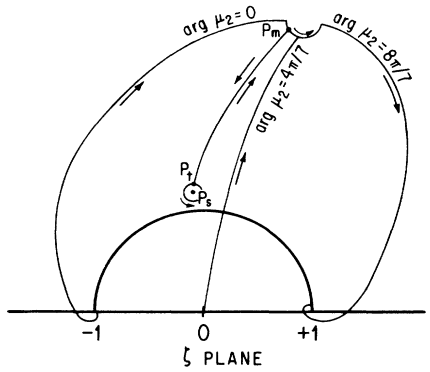

FIG. 2. Paths of integration for calculating the mismatch of the functions good at each tail. p_2 is the same as in Fig. 1.

Two things change when one of the quadrupole perturbations is added. One is we get an extra scattering. The second is that we have to deform the contour about the pole to stay on the right Riemann sheet. To evaluate (40) I will use steepest descent paths for the integrals.[29] There is an extra pole in R from τ, which leaves a residue when we wrap the contour around it. This is shown in Fig. 2. The net effect is that, as in the earlier case, we find that F_α is not scattered (so that $F_\alpha \sim g_\alpha$ globally again), while F_β does scatter. The new solution $f^{(-1)}$ good at the tail $\xi=-1$ differs from the old solution f that was good at the tail in the constant-τ case by an extra amount of F_α:

$$f^{(-1)} = f + M_L^{(-1)} F_\alpha , \tag{41}$$

where $M_L^{(-1)}$ is a constant I will calculate which comes from variations in τ between the tail $\xi=-1$ and the tip of the finger. Similarly, when we continue from the right side tail $\xi=1$ we get

$$f^{(+1)} = \tilde{f} - M_L^{(+1)} F_\alpha , \tag{42}$$

where $M_L^{(+1)}$ will be a constant that will come from perturbations to τ between the tail $\xi=1$ and the tip. The difference between them is then $f^{(-1)} - f^{(+1)} = (M_S + M_L^{(-1)} + M_L^{(+1)}) F_\alpha$ so matching reduces to

$$M_S + M_L = 0 , \tag{43}$$

where

$$M_L = M_L^{(-1)} + M_L^{(+1)} . \tag{44}$$

The mismatch that comes from the global shape of the finger is M_S, while M_L is the mismatch that comes from the local perturbations. The selection condition is (43): that the mismatch should vanish. The hard work ahead comes in calculating these constants.

D. Calculating M_S

I first consider M_S, as Tanveer essentially calculates it in his paper, and it will help to follow what he has done.

The calculation is going to get grungy, but there is really no way around that. There are two parts to the calculation. The first is to find the connection formulas for the F's, and the second is to evaluate the steepest descent integrals and residues around the poles. We begin with the connection formulas.

The connection formula problem has an extensive literature in applied mathematics.[30,31] It is most highly developed for second-order equations, both because it is the simplest equation with the connection problem, and because many of the most important differential equations in physics are second order. This is one complication in attempting to do this singular perturbation approach in the time-dependent case: there we are working with a third-order equation.[32] We will be using the technique of matched asymptotic expansions to get the connection formula in this paper. The idea is to look very near a singular point, where the differential equation looks quite simple, and then transform it into a form with special function solutions. From the known asymptotic properties of the special functions, we can then match to the far region WKBJ solutions and get the connection formula.

Near the turning point $\zeta=1/p_2$ Tanveer introduces the local variable

$$\mu_2=e^{i\pi/7}\delta_2^{2/7}(1+p_2\zeta)\ , \tag{45}$$

where

$$\delta_2=p_2^{3/2}(p_1+p_2)^{3/2}(1-p_2^2)^{-3/2}(1+p_1p_2)^{1/2}G^{-1}\ . \tag{46}$$

The resulting differential equation for μ_2 has two homogeneous solutions $\mu_2 K_{4/7}(4/7\mu_2^{7/4})$ and $\mu_2 K_{4/7}(4/7\mu_2^{7/4}e^{-i\pi})$, where $K_{4/7}$ are modified Bessel functions (MBF).[29] Using the asymptotic expansion for the MBF, that

$$K_\nu\sim\left[\frac{\pi}{2z}\right]^{1/2}e^{-z}\ \text{for}\ |z|\to\infty,\ |\arg(z)|<\frac{3\pi}{2}\ . \tag{47}$$

We can match these to the WKBJ solutions, so that

$$F_\beta\sim k_2 y_2^{4/7}K_{4/7}(y_2)\ , \tag{48}$$

$$F_\alpha\sim ik_2 y_2^{4/7}K_{4/7}(e^{-i\pi}y_2)\ , \tag{49}$$

where

$$y_2=\tfrac{4}{7}\mu_2^{4/7} \tag{50}$$

and

$$k_2=\pi^{-1/2}7^{1/14}2^{5/14}e^{-i11\pi/28}p_2^{1/14}(p_1+p_2)^{1/14}\times(1-p_2^2)^{-1/14}(1+p_1p_2)^{-1/7}G^{1/28}[\tau(-1/p_2)]^{-1/4} \tag{51}$$

(For the choice used here of $-1/p_2$ as the origin, since we are expanding about $-1/p_2$, the WKBJ integral factor $e^{P(-1/p_2)G^{-1/2}}$ is just 1.) We want to look at the asymptotic properties of the MBF for large arguments, so we require $\delta_2\gg 1$. Then the restrictions on the analysis are

$$\lambda\gg G \tag{52}$$

and

$$|p_2^{3/2}(p_1+p_2)^{3/2}|\gg G\ . \tag{53}$$

This latter restriction will be relevant when I consider the comparison with the simulation later on. Now the expansion (47) for K_ν is only valid for $|arg(y_2)|<3\pi/2$, or equivalently $|arg(\mu_2)|<6\pi/7$ for F_β, and $-2\pi/7<\arg(\mu_2)<10\pi/7$ for F_α. That means this expansion for F_α is valid in all three sectors 1, 2, and 3 (see Fig. 2), where $0<\arg(\mu_2)<8\pi/7$, while a new expansion is needed for F_β in sector 3. We again use the properties of MBF that

$$K_\nu=2\cos(\pi\nu)K_\nu(e^{\pm i\pi}z)-K_\nu(e^{\pm i2\pi}z) \tag{54}$$

and find that

$$F_\beta\sim g_\beta+2i\cos(4\pi/7)g_\alpha \tag{55}$$

in sector 3. These are our connection formulas, showing $F_\alpha\sim g_\alpha$ everywhere, and $F_\beta\sim g_\beta+b_m g_\alpha$ in 3, with

$$b_m=2i\cos(4\pi/7)\ . \tag{56}$$

Now to calculate M_S. Break up the paths of integration as Tanveer does into steepest descent paths and arcs around poles. The constant ImP paths connecting $\zeta=-1$ to $\zeta=1$ are through the singularity $-1/p_2$. We deform the contour to go along these legs. The line from $\zeta=-1$ comes in on $\arg(\mu_2)=0$, the line from $\zeta=0$ on $\arg(\mu_2)=4\pi/7$, and the line from $\zeta=1$ comes in on $\arg(\mu_2)=8\pi/7$ (see Fig. 2). It will turn out there is a pole at $\mu_2=0$ in the integrals, so we connect the steepest descent lines with a circular arc of radius ϵ. The drop-off point p_m can lie anywhere on our path through sector 1; let it be at ϵe^{im}. Then

$$\begin{aligned}M_S&=b_m\int_0^{p_m}d\zeta' F_\alpha\frac{R}{W}-\int_{-1}^{p_m}d\zeta' F_\beta\frac{R}{W}-\int_{p_m}^{1}d\zeta'\tilde F_\beta\frac{R}{W}\\&=b_m\int_0^{\epsilon e^{im}}F_\alpha-\int_{-1}^{\epsilon e^{i0}}F_\beta-\int_{\epsilon e^{i0}}^{\epsilon e^{im}}F_\beta-\int_1^{\epsilon e^{i8\pi/7}}\tilde F_\beta-\int_{\epsilon e^{i8\pi/7}}^{\epsilon e^{im}}\tilde F_\beta\\&=-\int_{\epsilon e^{i0}}^{\epsilon e^{i4\pi/7}}F_\beta-\int_{\epsilon e^{i8\pi/7}}^{\epsilon e^{i4\pi/7}}\tilde F_\beta+\left[b_m\int_0^{\epsilon e^{i4\pi/7}}F_\alpha-\int_{-1}^{\epsilon e^{i0}}F_\beta-\int_1^{\epsilon e^{i8\pi/7}}\tilde F_\beta\right]\\&\quad+\left[b_m\int_{\epsilon e^{i4\pi/7}}^{\epsilon e^{im}}F_\alpha+\int_{\epsilon e^{i4\pi/7}}^{\epsilon e^{im}}\tilde F_\beta-\int_{\epsilon e^{i4\pi/7}}^{\epsilon e^{im}}F_\beta\right].\end{aligned} \tag{57}$$

(For the symbolic integrals written here, the limits of integration are in the variable μ_2.) Using the connecting formula, the steepest descent integrals in the first bracket cancel, and the arc integrals in the second bracket cancel as well. As advertised, the result is independent of the lower limit $\zeta_\alpha=0$ in (35) and where we choose p_m to be. Near $\zeta=-1/p_2$

$$\frac{R}{W}=\frac{iG^{1/2}p_2}{2(1+p_2\zeta)} . \tag{58}$$

For $|z|\to 0$

$$K_\nu(z)\sim\tfrac{1}{2}\Gamma(\nu)(\tfrac{1}{2}z)^{-\nu} . \tag{59}$$

Then

$$\begin{aligned} M_S=&\int_{\epsilon e^{i0}}^{\epsilon e^{i4\pi/7}} k_2 y_2^{4/7}\tfrac{1}{2}\Gamma(\tfrac{4}{7})(\tfrac{1}{2}y_2)^{-4/7}\frac{iG^{1/2}}{2}\frac{d\mu_2}{\mu_2} \\ &+\int_{\epsilon e^{i8\pi/7}}^{\epsilon e^{i4\pi/7}} e^{-i\pi}k_2 y_2^{4/7}\tfrac{1}{2}\Gamma(\tfrac{4}{7})(\tfrac{1}{2}y_2 e^{-i2\pi})^{-4/7} \\ &\times\frac{iG^{1/2}}{2}\frac{d\mu_2}{\mu_2} \\ =&G^{1/2}k_2\Gamma(\tfrac{4}{7})\pi\frac{2^{4/7}}{7}(1+e^{i\pi/7}) . \end{aligned} \tag{60}$$

IV. NONCONSTANT τ

In this section I calculate the contributions of the nonconstant τ to the mismatch at the tip of the solutions good at each tail. This is done explicitly for one quadrupole, and more generally for multiple quadrupoles.

A. Calculating M_L

The mismatch term M_L is clearly dependent on τ. Let us do it first for a single quadrupole, and then later show how to incorporate many of them. To calculate the scattering, I will make the first and only inconsistency of this whole calculation: I assume that the zeros and poles are isolated, that is, that G is small enough so that they can be treated separately. This turns out not to be true, at least in the regimes in which we will be most interested. However, most likely the answer would only change in a slight quantitative way, and when I compare the theory to a numerical simulation it will be seen that there already is very good quantitative agreement. Another reason to present it this way is it is the easiest conceptually.

1. Sectors of τ

Near the zero of $1/\tau$, we have

$$f''+Q_t f'+L_t\frac{\zeta-p_t}{G}tf=R_t , \tag{61}$$

where the subscript denotes the functions evaluated at $p_t=\zeta_0(1+\sigma)$ [for example, $R_t=R(p_t)$]. Also, $1/\tau(p_t)\equiv(\zeta-p_t)t$. Changing variables in this neighborhood of p_t, we see the $Q_t f'$ term is small compared to the others, and we drop it. That leaves, for the homogeneous part, Airy's equation. Two solutions are

$$\begin{aligned} &\mathrm{Ai}\left[\left[\frac{e^{-i\pi}L_t t}{G}\right]^{1/3}(\zeta-p_t)\right] \\ &\mathrm{Ai}\left[\left[\frac{e^{-i\pi}L_t t}{G}\right]^{1/3}(\zeta-p_t)e^{-i2\pi/3}\right] . \end{aligned} \tag{62}$$

Airy functions also have a MBF representation

$$\mathrm{Ai}(z)=\frac{1}{\pi}\left[\frac{z}{3}\right]^{1/2}K_{1/3}(\tfrac{2}{3}z^{2/3}) . \tag{63}$$

More generally, for differential equations of the form

$$f''+cy^\alpha f=0 \tag{64}$$

make the ansatz $f=y^a K_\nu(by^d)$. Then it can be shown that these trial solutions do indeed work with

$$f=y^{1/2}K_{1/(\alpha+2)}\left[\frac{2}{\alpha+2}e^{\pm i\pi/2}c^{1/2}y^{(\alpha+2)/2}\right] . \tag{65}$$

This is the form of the equation for any isolated singularity of τ, and thus all that is needed are the properties of MBF under the approximation, which is made in this paper, that the singularities are isolated. Observe that dropping the first derivative term Qf' was justified, since in the small parameter G this term is of order $G^{-1/2}$ while f'' and cf are of order G^{-1}. The next task is to study the arguments of the MBF's around the two types of singularities of the quadrupole so the scattering can be found.

First, take a simplified version of the perturbation, a dipole $1/\tau=T=\zeta/(1+\zeta)$. Near the zero at $\zeta=0$, ignoring L (i.e., $L=1$), the form of P is $P\sim\int^\zeta T^{1/2}d\zeta'\sim\zeta^{3/2}$, so there will be three lines of constant real part coming out, and three of constant imaginary part emanating from the zero. Similarly, near $\zeta=-1$ we get $P\sim(1+\zeta)^{1/2}$ so there is just one constant real and one constant imaginary line coming out at this pole. The Stokes and anti-Stokes lines are shown in Fig. 3, with a branch cut in between 0 and -1. Note that far away $T\cong 1$ so it should look like $P\sim\zeta$, so the constant ReP lines are parallel to the real axis. Now put L back in. This local perturbation T has to be embedded in the field due to L. That means rotating the dipole $\pi/2$ to line up the increasing ReP lines; that is, for a perturbation at the tip, and a symmetric finger. In the more general case, there will be a slight shear as well. When it is sheared, the branch cut from the zero and pole splits.

For the quadrupole, there are two cases, for $A<0$ and for $A>0$. For $A<0$ the pole of τ will be closer to the unit circle than the zero as depicted in Fig. 4(a). For $A>0$ we get Fig. 4(b). Now observe the Stokes lines from the dipole below the unit circle; if they cross the circle, they do it twice, so that the two tails of the finger, at $\zeta=\pm 1$, are in the same sector. Thus there will be no scattering from the bottom dipole. Also, when we deform the integral along the finger onto the steepest descent paths, we do not go around these singularities below

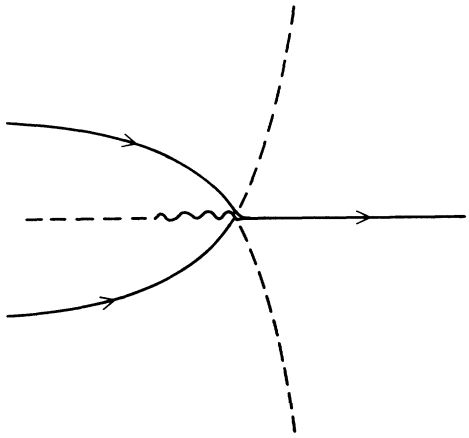

FIG. 3. Stokes lines (dashed) and anti-Stokes lines (solid) for the simple dipole $P=\int^{\zeta}[\zeta'/(1+\zeta')]^{1/2}d\zeta'$. The wavy line is a branch cut. The arrows are in the direction of increasing value.

the unit circle. For simplicity, then, I will no longer discuss the bottom dipole in the calculation, as its structure does not enter into the problem. The next point is a bit more subtle and interesting. Observe that the branch cuts could have been drawn in a different way so that the result for $A<0$ looked like Fig. 5(a) and that for $A>0$ like Fig. 5(b). The physics better not depend on this arbitrary choice. Let us study the $A<0$ problem to see that it indeed does not. To show that the results turn out the same, we have to calculate $M_L^{(-1)}$.

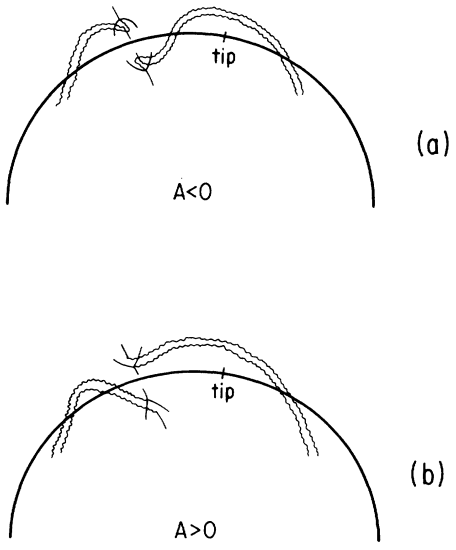

FIG. 4. Schematic figure of the branch cuts from a quadrupole perturbation. The anti-Stokes lines are solid, the branch cuts are wavy. Scattering from p_t after going around p_s (a) $A<0$, (b) $A>0$.

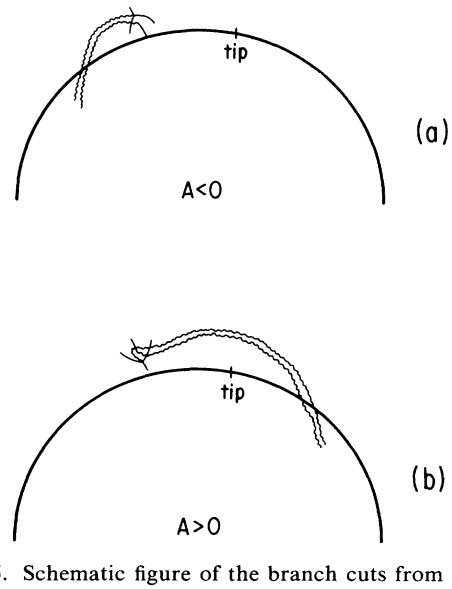

FIG. 5. Schematic figure of the branch cuts from a quadrupole perturbation. The anti-Stokes lines are solid, the branch cuts are wavy. Scattering from p_t before going around p_s. (a) $A<0$, (b) $A>0$.

2. *Branch cut independence*

In this section I calculate $M_L^{(-1)}$ for an $A<0$ quadrupole, and show that it does not depend on how the branch cuts are made. To see what the scattering will be from the singularities, we now study the arguments of the MBF for the two different ways of making the branch cuts. From the directions of the arrows, we can fix what the arguments are. Each Stokes line corresponds to a change of the argument of the MBF by π. The arrows are in the direction where g_β is becoming exponentially small. That means for $g_\beta \sim k_t\sqrt{\zeta-p_t}K_{1/3}(y_t)$, using (47), that $\arg(y_t)=2n\pi$ on the lines with arrows pointing away from p_t. The branch cuts are at $\arg(y_t)=\pm 3\pi/2$. Our two cases are Fig. 4(a) and Fig. 5(a). On the line coming down in case I, $\arg(y_t)=0$, while in case II, $\arg(y_t)=-2\pi$. Note the order that the cuts cross the circle: when continuing from the tail to the tip, in case I our contour will go around p_s before scattering from p_t, while in case II it will scatter from p_t before going around p_s.

First I calculate the scattering. Using the solutions found previously, before scattering

$$F_\beta \sim k_t \frac{1}{E_t}\sqrt{\zeta-p_t}K_{1/3}(y_t)\ , \tag{66}$$

where k_t is a local algebraic constant, y_t the local scaled variable, and

$$E_t=\exp\left[G^{-1/2}\int_{-1/p_2}^{p_t} iL^{1/2}\tau^{-1/2}d\zeta'\right]\ , \tag{67}$$

the WKBJ integral. Now, using properties of the MBF, we get

$$F_\alpha \sim e^{\pm i\pi/2} k_t E_t \sqrt{\zeta - p_t}\, K_{1/3}(y_t e^{\pm i\pi}) \ . \tag{68}$$

Define $\hat{F}_\beta \sim g_\beta$ after passing through the scattering. Then use

$$K_{1/3}(y) = K_{1/3}(y e^{\pm i\pi}) - K_{1/3}(y e^{\pm i2\pi}) \ . \tag{69}$$

In case I, we get that $\arg(y_t)$ goes from 0 on the line of the contour path into p_t to 2π on the line out of p_t after scattering. Therefore

$$\begin{aligned} F_\beta &\sim k_t \frac{1}{E_t} \sqrt{\zeta - p_t}\, K_{1/3}(y_t) \ , \\ \hat{F}_\beta^I &\sim -k_t \frac{1}{E_t} \sqrt{\zeta - p_t}\, K_{1/3}(y_t e^{-i2\pi}) \ , \\ F_\alpha &\sim e^{-i\pi/2} k_t \frac{1}{E_t} \sqrt{\zeta - p_t}\, K_{1/3}(y_t e^{-i\pi}) \ . \end{aligned} \tag{70}$$

Thus

$$F_\beta \sim \hat{F}_\beta^I + i E_t^{-2} F_\alpha \tag{71}$$

after scattering. In case II, we get that $\arg(y_t)$ goes from -2π to 0. Therefore

$$\begin{aligned} F_\beta &\sim -k_t \frac{1}{E_t} \sqrt{\zeta - p_t}\, K_{1/3}(y_t e^{i2\pi}) \ , \\ \hat{F}_\beta^{\rm II} &\sim k_t \frac{1}{E_t} \sqrt{\zeta - p_t}\, K_{1/3}(y_t) \ , \\ F_\alpha &\sim e^{i\pi/2} k_t \frac{1}{E_t} \sqrt{\zeta - p_t}\, K_{1/3}(y_t e^{i\pi}) \ , \end{aligned} \tag{72}$$

and again

$$F_\beta \sim \hat{F}_\beta^{\rm II} + i E_t^{-2} F_\alpha \ . \tag{73}$$

Therefore in both cases, after scattering,

$$F_\beta \sim g_\beta + b_t g_\alpha \tag{74}$$

where

$$b_t = i E_t^{-2} \ . \tag{75}$$

Now let us evaluate $M_L^{(1-)}$. We have to be careful to go around the poles in the same order as we would if we went along the finger on the unit circle from the $\zeta = -1$ tail to the tip. So we need to be able to keep track of what Riemann sheet we are on. Denote $\zeta^{(-1)}$ the ζ that is on the same Riemann sheet as the tail at -1, and $\zeta^{(-0)}$ the ζ that is on the same sheet as the tip, before scattering at p_m. For one quadrupole between $\zeta = -1$ and the tip, and case I with scattering at p_t after passing around p_s

$$\begin{aligned} f^{(-1)} &= F_\beta \int_0^{\zeta^{(-1)}} d\zeta' F_\alpha \frac{R}{W} - F_\alpha \int_{-1}^{\zeta^{(-1)}} d\zeta' F_\beta \frac{R}{W} \\ &= (\hat{F}_\beta^I + b_t F_\alpha) \left[\int_0^{\zeta^{(-0)}} F_\alpha - \oint_{p_s} F_\alpha \right] \\ &- F_\alpha \left[\int_{-1}^{p_m^{(-1)}} F_\beta + \int_{p_m^{(-1)}}^{p_t^{(-1)}} F_\beta + \oint_{p_s} F_\beta + \int_{p_t^{(-0)}}^{\zeta^{(-0)}} b_m F_\alpha + \int_{p_t^{(-0)}}^{p_m^{(-0)}} \hat{F}_\beta^I + \int_{p_m^{(-0)}}^{\zeta^{(-0)}} \hat{F}_\beta^I \right] \\ &= \hat{F}_\beta^I \int_0^{\zeta^{(-0)}} F_\alpha - F_\alpha \left[\int_{-1}^{p_m^{(-1)}} F_\beta + \int_{p_m^{(-0)}}^{\zeta^{(-0)}} \hat{F}_\beta^I \right] \\ &+ F_\alpha \left[\int_0^{p_t^{(-0)}} b_t F_\alpha - b_t \oint_{p_s} F_\alpha - \int_{p_m^{(-1)}}^{p_t^{(-1)}} F_\beta - \oint_{p_s} F_\beta - \int_{p_t^{(-0)}}^{p_m^{(-0)}} \hat{F}_\beta^I \right] \\ &= f^{(-0)} + M_L^{(-1)} F_\alpha \ . \end{aligned} \tag{76}$$

Here $f^{(-0)}$ is equal to the f we had from the constant-τ case, since both F_β and $\hat{F}_\beta^I$ are asymptotic to g_β on the respective sheets. Now evaluating $M_L^{(-1)}$, from the connection formula, we find that the straight line integrals cancel:

$$\int_0^{p_t^{(-0)}} b_t F_\alpha - \int_{p_m^{(-1)}}^{p_t^{(-1)}} F_\beta - \int_{p_t^{(-0)}}^{p_m^{(-0)}} \hat{F}_\beta^I = 0 \ . \tag{77}$$

This cancellation is more apparent when a steepest descent approximation is made on the integrals and their asymptotic representation near p_t is examined. Near p_t, R_t is a constant (h, h', and I_2 are slowly varying there) as is W_t, so we can pull them out of the integral. (The subscripts on R and W denotes evaluation at p_t.) Dropping the constants, we get

$$\int_0^{p_t^{(-0)}} b_t F_\alpha - \int_{p_m^{(-1)}}^{p_t^{(-1)}} F_\beta - \int_{p_t^{(-0)}}^{p_m^{(-0)}} \hat{F}_\beta^I \sim \int_{\infty e^{i\pi}}^{\epsilon e^{i\pi}} dy\, K_{1/3}(y e^{-i\pi}) - \int_{\infty e^{i0}}^{\epsilon e^{i0}} dy\, K_{1/3}(y) - \int_{\infty e^{i2\pi}}^{\epsilon e^{i2\pi}} dy\, K_{1/3}(y e^{-i2\pi}) = 0 \ . \tag{78}$$

Thus

$$M_L^{(-1)} = -b_t \oint_{p_s} d\zeta' F_\alpha \frac{R}{W} - \oint_{p_s} d\zeta' F_\beta \frac{R}{W} \ . \tag{79}$$

That was for case I. For case II, we have

$$f=(\hat{F}_\beta^{\mathrm{II}}+b_t F_\alpha)\left[\int_0^{\zeta^{(-0)}} F_\alpha-\oint_{p_s} F_\alpha\right]$$
$$-F_\alpha\left[\int_{-1}^{p_m^{(-1)}} F_\beta+\int_{p_m^{(-1)}}^{p_t^{(-1)}} F_\beta+\oint_{p_s} b_t F_\alpha+\int_{p_t^{(-0)}}^{\zeta^{(-0)}} b_t F_\alpha+\oint_{p_s}\hat{F}_\beta^{\mathrm{II}}+\int_{p_t^{(-0)}}^{p_m^{(-0)}}\hat{F}_\beta^{\mathrm{II}}+\int_{p_m^{(-0)}}^{\zeta^{(-0)}}\hat{F}_\beta^{\mathrm{II}}\right]$$
$$=f+M_{L\,\mathrm{II}}^{(-1)}F_\alpha\ , \tag{80}$$

where

$$M_{L\,\mathrm{II}}^{(-1)}=b_t\int_0^{p_t^{(-0)}} F_\alpha-2b_t\oint_{p_s}F_\alpha-\int_{p_m^{(-1)}}^{p_t^{(-1)}}F_\beta-\oint_{p_s}\hat{F}_\beta^{\mathrm{II}}-\int_{p_t^{(-0)}}^{p_m^{(-0)}}\hat{F}_\beta^{\mathrm{II}}\ . \tag{81}$$

In the same way as before, the straight line integrals cancel. Then

$$M_{L\,\mathrm{II}}^{(-1)}=-2b_t\oint_{p_s}F_\alpha-\oint_{p_s}\hat{F}_\beta^{\mathrm{II}}=-b_t\oint_{p_s}F_\alpha-\oint_{p_s}F_\beta\ , \tag{82}$$

which is the same as before. I have shown that case I and II give the same results, so from now on I will use case I, the one on which we go around the pole before scattering.

3. *Multiple Quadrupoles*

Now let's generalize the result to handle multiple $A<0$ quadrupoles on the finger. I will first consider the case of two quadrupoles and then show how to generalize further. Let $F_\beta\sim F_\beta^{2-}+b_{2-}F_\alpha$ be the scattering at the zero p_t^{2-} and $F_\beta^{2-}\sim F_\beta^{1-}+b_{1-}F_\alpha$ be the scattering at the zero p_t^{1-}. Then $F_\beta\sim F_\beta^{(-0)}+b_-F_\alpha$ near the tip at $\zeta^{(-0)}$, where $b_-=b_{2-}+b_{1-}$ and $F_\beta^{(-0)}\sim g_\beta$. Then

$$f^{(-1)}=(\hat{F}_\beta^{(-0)}+b_tF_\alpha)\left[\int_0^{\zeta^{(-0)}}F_\alpha-\oint_{p_s^{2-}}F_\alpha-\oint_{p_s^{1-}}F_\alpha\right]$$
$$-F_\alpha\left[\int_{-1}^{p_m^{(-1)}}F_\beta+\int_{p_m^{(-1)}}^{p_t^{2-}}F_\beta+\oint_{p_s^{2-}}F_\beta+\int_{p_t^{2-}}^{p_m^{2-}}+\int_{p_t^{2-}}^{\zeta^{2-}}b_{2-}F_\alpha\right.$$
$$\left.+\int_{p_m^{2-}}^{p_t^{1-}}F_\beta^{2-}+\oint_{p_s^{1-}}F_\beta^{2-}+\int_{p_t^{1-}}^{p_m^{(-0)}}F_\beta^{1-}+\int_{p_t^{1-}}^{\zeta^{1-}}b_{1-}F_\alpha+\int_{p_m^{(-0)}}^{\zeta^{(-0)}}F_\beta^{1-}\right]$$
$$=f^{(-0)}+M_{L\,2}^{(-1)}F_\alpha\ , \tag{83}$$

where

$$M_{L\,2}^{(-1)}=-\oint_{p_s^{2-}}b_{2-}F_\alpha-\oint_{p_s^{2-}}b_{1-}F_\alpha-\oint_{p_s^{2-}}F_\beta-\oint_{p_s^{1-}}b_{1-}F_\alpha-\oint_{p_s^{1-}}F_\beta^{2-}$$
$$=-\oint_{p_s^{2-}}F_\beta-\oint_{p_s^{1-}}F_\beta-b_2\left[\oint_{p_s^{2-}}F_\alpha-\oint_{p_s^{1-}}F_\alpha\right]-b_{1-}\left[\oint_{p_s^{2-}}F_\alpha+\oint_{p_s^{1-}}F_\alpha\right]\ . \tag{84}$$

Generalize (84) to an arbitrary number of wires; we get a $\oint F_\beta$ for each p_s and a $-b\oint F_\alpha$ but with a plus or minus sign depending on whether the particular coefficient scattered before or after going around the pole in question. The contributions of the quadrupoles are summarized as follows:

$$M_L^{(-1)}=\sum_k^{n-}\sum_j^{n-}-\oint_{p_s^k}d\zeta' F_\beta\frac{R}{W}-\epsilon_{kj}b_j\oint_{p_s^k}d\zeta' F_\alpha\frac{R}{W}\ , \tag{85}$$

where

$$\epsilon_{kj}=\begin{cases}1 & \text{if } |j|\le|k|\\ -1 & \text{if } |j|>|k|\end{cases} \tag{86}$$

and

$$b_j=iE_j^{-2}\ , \tag{87}$$

with

$$E_j=i\exp\left[G^{-1/2}\int_{-1/p_2}^{p_t^j} iL^{1/2}\tau^{-1/2}d\zeta'\right]\ . \tag{88}$$

Let us calculate $M_L^{(+1)}$ for the case of just one quadrupole between the tip and the $\zeta=1$ tail,

$$\tilde{f}=\tilde{F}_\beta\int_0^{\zeta^{(+1)}}F_\alpha-F_\alpha\int_{-1}^{\zeta^{(+1)}}\tilde{F}_\beta$$
$$=(F_\beta^{(+0)}+b_+F_\alpha)\left[\int_0^{\zeta^{(+0)}}F_\alpha+\oint_{p_s}F_\alpha\right]$$
$$-F_\alpha\left[\int_1^{p_m^{(+1)}}\tilde{F}_\beta+\int_{p_m^{(+1)}}^{p_t^{(+1)}}\tilde{F}_\beta-\oint_{p_s}\tilde{F}_\beta+\int_{p_t^{(+0)}}^{\zeta^{(+0)}}b_+F_\alpha+\int_{p_t^{(+0)}}^{p_m^{(+0)}}F_\beta^{(+0)}+\int_{p_m^{(+0)}}^{\zeta^{(+0)}}F_\beta^{(+0)}\right]$$
$$=f^{(+0)}+M_L^{(+1)}F_\alpha\ , \tag{89}$$

where

$$M_L^{(+1)}=-\oint_{p_s}\tilde{F}_\beta-\oint_{p_s}b_+F_\alpha\ . \tag{90}$$

The only difference between $M_L^{(+1)}$ and $M_L^{(-1)}$ is in the sign of the terms. There is an extra minus sign in the b's: $B_+=-iE_{t+}^{-2}$. That done, we have

$$M_L^{(+1)}=\sum_k^{n+}\sum_j^{n+}-\oint_{p_s^k}d\zeta' F_\beta\frac{R}{W}-\epsilon_{kj}b_j\oint_{p_s^k}d\zeta' F_\alpha\frac{R}{W}\ , \tag{91}$$

where

$$b_j=-iE_j^{-2}\quad\text{for } j=n+ \tag{92}$$

and ϵ_{kj} is the same as (86).

4. *Evaluating a single quadrupole*

Finally, let us evaluate the expression for a single quadrupole. We are left with M_L being integrals around the poles. Near p_s, R is dominated by the pole of $1/\tau$, so that

$$R_s=-L_s s\frac{1}{\zeta-p_s}f_1\left[\frac{1}{p_s}\right], \tag{93}$$

where

$$\frac{1}{\tau(1/p_s)}\equiv s\frac{1}{\zeta-p_s} \tag{94}$$

and as was the convention before, with the subscript s denoting evaluation at $\zeta=p_s$.

$$\frac{R_s}{W_s}=-G^{-1/2}\frac{i}{2}|h_s|f_1\left[\frac{1}{p_s}\right]\frac{s}{p_s}\frac{1}{\zeta-p_s}\ . \tag{95}$$

What about F_α and F_β? First, I will treat the case of $A<0$. We will then see how the result is modified for $A>0$.

For $A<0$,

$$F_\beta\sim k_s(\zeta-p_s)^{1/2}K_1(y_s)E_s^{-1} \tag{96}$$

where

$$y_s=\left[\frac{e^{-i\pi}Ls}{G}\right]^{1/2}(\zeta-p_s)^{1/2} \tag{97}$$

$$k_s=2\pi^{-1/2}e^{-i\pi/4}h_s^{1/2}G^{-1/4} \tag{98}$$

and E_s is the WKBJ integral evaluated at p_s. For $A<0$, ReP is larger at p_t than at p_s. So the argument of y_s on the anti-Stokes line is 0. For perturbations between $\zeta=-1$ and the tip, $\arg(y_s)\in(-\pi,\pi/2)$. That means on the contour path around p_s

$$F_\alpha\sim e^{i\pi/2}k_s(\zeta-p_s)^{1/2}K_1(y_s e^{i\pi})E_s\ . \tag{99}$$

So $\arg(y_s e^{i\pi})\in(0,3\pi/2)$ and neither F_α nor F_β scatter. Alternatively, for perturbations between the tail $\zeta=1$ and the tip, $\arg(y_s)\in(\pi,-\pi/2)$ so

$$F_\alpha\sim e^{-i\pi/2}k_s(\zeta-p_s)^{1/2}K_1(y_s e^{-i\pi})E_s\ . \tag{100}$$

Using the asymptotic properties of MBF for $|z|\to\infty$ we find in both cases that

$$b_t F_\alpha\sim\frac{E_s^2}{E_t^2}F_\beta\ . \tag{101}$$

So

$$M_L^{(\pm1)}=-\oint_{p_s}d\zeta' F_\beta\left[1+\frac{E_s^2}{E_t^2}\right]\frac{R}{W}\ . \tag{102}$$

Now

$$F_\beta\sim k_s\left[\frac{e^{-i\pi}Ls}{G}\right]^{-1/2}E_s^{-1} \tag{103}$$

at p_s, which is just a constant. So the integral around p_s is a simple residue of R_s:

$$M_L^{(\pm1)}=-G^{-3/4}\pi^{1/2}|h_s|^{1/2}f_1\left[\frac{1}{p_s}\right]e^{i\pi/4}$$
$$\times\left[\frac{s}{p_s}\right]^{1/2}E_s^{-1}\left[1+\frac{E_s^2}{E_t^2}\right]\ . \tag{104}$$

The expression

$$\frac{s}{p_s}=\frac{r_s-r_t}{r_s}\frac{r_s-1/r_t}{r_s-1/r_s} \tag{105}$$

for small σ and σA is to lowest order

$$\frac{s}{p_s}\cong\frac{A\sigma}{2\sqrt{1+A}}\ . \tag{106}$$

For $A>0$ things are a bit different. Keeping the convention that we go around the pole before scattering, we have the cuts looking like Fig. 4(b). Now things are a little backwards, in that perturbations placed between the -1 tail and the tip have their cuts cross the unit circle on the right. That means

$$b_j=\begin{cases}-iE_j^{-2} & \text{for } j_+\\ iE_j^{-2} & \text{for } j_-\end{cases},\quad A>0\ . \tag{107}$$

For perturbations between the -1 tail and the tip, F_β is as in (96) with $\arg(y_s)\in(-3\pi/2,0)$. On the other side, though,

$$F_\beta \sim e^{i\pi} k_s (\zeta - p_s)^{1/2} K_1(y_s e^{i2\pi}) E_s^{-1} , \tag{108}$$

with $\arg(y_s)\in(3\pi/2,0)$. In both cases (99) holds, with $\arg(y_s e^{i\pi})\in(-\pi/2,\pi)$ for -1 to the tip, and $\arg(y_s e^{i\pi})\in(\pi/2,-\pi)$ for the other side. Once again (101) holds. What changes is $\oint_{p_s} F_\beta$: now there is a difference between evaluating it on the right versus the left. There is a minus sign between them, with

$$F_\beta \sim \begin{cases} k_s \left[\dfrac{e^{-i\pi} Ls}{G}\right]^{-1/2} E_s^{-1} & \text{for } \beta_+ \\ -k_s \left[\dfrac{e^{-i\pi} Ls}{G}\right]^{-1/2} E_s^{-1} & \text{for } \beta_- \end{cases} , \quad A>0 . \tag{109}$$

Our result for one quadrupole per side, valid for all A, is:

$$M_\tau = G^{-3/4}\pi^{1/2}|h_s|^{1/2} f_1\left[\frac{1}{p_s}\right] e^{i\pi/4} \times \left[\frac{s}{p_s}\right]^{1/2} E_s^{-1}\left[1+\frac{E_s^2}{E_t^2}\right] , \tag{110}$$

$$M_L^{(-1)} = M_\tau , \tag{111}$$

$$M_L^{(+1)} = -M_\tau \operatorname{sgn}(A) , \tag{112}$$

where

$$\operatorname{sgn}(A) = \frac{A}{|A|} . \tag{113}$$

5. General expression

Finally, I summarize the results valid for all A:

$$M_L = \sum_k^{n-,m+} \sum_j^{n-,m+} - \oint_{p_s^k} d\zeta' F_\beta \frac{R}{W} - \epsilon_{kj} b_j \oint_{p_s^k} d\zeta' F_\alpha \frac{R}{W} , \tag{114}$$

where

$$\epsilon_{kj} = \begin{cases} 1 & \text{if } |j|\le|k| \\ -1 & \text{if } |j|>|k| \end{cases} , \tag{115}$$

$$b_j \sim \begin{cases} -iE_j^{-2}\operatorname{sgn}(A) & \text{for } j_+ \\ iE_j^{-2}\operatorname{sgn}(A) & \text{for } j_- \end{cases} . \tag{116}$$

B. Simplifying general expression and method

1. Physical interpretation of WKBJ solutions

Let us try to get some feel for what the results mean. If we change into the more physical variables l and θ, with l the arclength along the interface, and θ the angle the normal to the interface makes with the axis down the length of the channel, then (18) becomes

$$f_{ll} + (1-e^{-i\theta})\frac{de^{i\theta}}{dl} f_l + \frac{\pi^2}{4G\tau} e^{i\theta} f = \left[\frac{d\zeta}{dl}\right]^2 R \tag{117}$$

and the WKBJ solutions

$$g_\alpha = e^{i\theta/4}\left[\frac{\pi^2}{4\tau}\right]^{-1/4} e^{e^{i\theta}} \times \exp\left[\frac{\pi}{2G^{1/2}}\int^l ie^{i\theta/2}\tau^{-1/2}dl'\right] , \tag{118}$$

$$g_\beta = e^{i\theta/4}\left[\frac{\pi^2}{4\tau}\right]^{-1/4} e^{e^{i\theta}} \times \exp\left[-\frac{\pi}{2G^{1/2}}\int^l ie^{i\theta/2}\tau^{-1/2}dl'\right] . \tag{119}$$

Bensimon, Pelce, and Shraiman[32] (BPS) have given a quite elegant interpretation of these functions. One looks for the modes $\xi = e^{ik(l)l+\omega t}$ which are marginally stable (i.e., with $\omega=0$) on a curved front with surface tension. As is usual with WKBJ, we assume θ is a slowly varying function of l on the length scale of $G^{1/2}$. It is quite straightforward to generalize their derivation to allow for nonconstant τ. The resulting marginal modes are

$$e^{-i\theta/4}\left[\frac{\pi^2}{4\tau}\right]^{-1/4} \exp\left[\pm\frac{\pi}{2G^{1/2}}\int^l ie^{i\theta/2}\tau^{-1/2}dl'\right] , \tag{120}$$

which are the same as (118) and (119) in the dominant exponential order, and the same in the algebraic order when θ is small.

2. Exponentially small contribution of far quadrupoles

In the experiments, wires far from the tip had no observable effect on the selection. This result can be seen (104) and (118): The contribution to M_L for a perturbation away from the tip becomes exponentially small. At a position l on the interface, it has decreased by

$$\exp\left[-G^{-1/2}\int^l \sin(\theta/2)dl'\right] .$$

Thus I can drastically simplify (114) when the separation of the quadrupoles is large. For a separation d, we need only consider the quadrupole closest to the tip on either side when

$$d \gtrsim G^{1/4} . \tag{121}$$

This is the loosest limit, and is found by taking θ small. Even tighter bounds can be obtained when θ is bigger.

V. RESULTS

A. Analytic results

Symmetry relations and scalings for selection are derived. The expressions for quadrupole perturbations derived in the previous parts are used, and then the results are shown to be more general.

1. Summary of equations to be used

Let us summarize the expression found in the previous section which I will be using here. The selection condition is that the mismatch at the tip of the two solutions good at each tail vanish:

$$M_S + M_L = 0 \ . \tag{122}$$

The global contribution to the mismatch from the finger shape is M_S. The local contributions from perturbations M_L is made up of two parts: contributions between the tip and the lower tail of the finger $M_L^{(-1)}$, and contributions between the upper tail and tip $M_L^{(+1)}$.

$$M_S = G^{1/2} k_2 \Gamma(\tfrac{4}{7}) \pi \frac{2^{11/7}}{7} \cos\left[\frac{\pi}{14}\right] e^{i\pi/14} \ , \tag{123}$$

where

$$k_2 = \pi^{-1/2} 7^{1/14} 2^{5/14} e^{-i\pi 11/28} p_2^{1/14} (p_1+p_2)^{1/14} \times (1-p_2^2)^{1/14} (1+p_1 p_2)^{-1/7} G^{1/28} \tau^{-1/4}\left[\frac{-1}{p_2}\right] , \tag{124}$$

For τ a quadrupole between the lower tail and tip given by (23), (27), and (28), and for $\sigma, \sigma A \ll 1$ we have

$$M_L^{(-1)} = -G^{3/4}\left[\frac{\sigma A}{2\sqrt{1+A}}\right]^{1/2} f_1\left[\frac{1}{p_s}\right] \pi^{1/2} \times |h_s|^{1/2} e^{i\pi/4} \frac{1}{E_s}\left[1+\frac{E_s^2}{E_t^2}\right] . \tag{125}$$

The term $|h_s|$ is $|h|$ evaluated at the pole $p_s = \zeta_0 r_s$, and E_s and E_t are the WKBJ integrals, with

$$E_s = \exp(P_s) = \exp\left[G^{-1/2} \int_{-1/p_2}^{p_s} iL^{1/2} \tau^{-1/2} d\zeta'\right] \tag{126}$$

and E_t the same but with the upper limit of the integration p_t. For a quadrupole between the tip and the other tail, $M_L^{(+1)}$ has the same form as $M_L^{(-1)}$ for $A<0$, but when $A>0$ there is an extra minus sign.

I now use these expressions to derive some analytic results. As we saw in Sec. IV B 2, the quadrupole closest to the tip dominates the selection when (121) holds. Thus the following sections hold more generally when there are additional quadrupoles away from the tip.

2. Symmetric and asymmetric solutions

The first thing to notice are the phases. The symmetry of the solution will be found by matching the phases of the terms. For $A<0$,

$$\arg(M_S) = -\pi\tfrac{4}{14} + \pi\tfrac{1}{14}[\arg(p_2) - \arg(1-p_2^2)] - \tfrac{1}{4}\arg[\tau(-1/p_2)] \ . \tag{127}$$

For a symmetric finger and a symmetric perturbation,

$$\arg(M_S) = -\frac{\pi}{4} \ . \tag{128}$$

Consider a symmetric τ with on quadrupole on each side of the tip. Then

$$\arg(M_L^{(-1)} + M_L^{(+1)}) = \frac{\pi}{4} + \frac{1}{2}\arg(A) + \arg\left[f_1\left[\frac{1}{p_2}\right]\frac{1}{E_s}\left[1+\frac{E_s^2}{E_t^2}\right] \pm f_1^*\left[\frac{1}{p_2}\right]\frac{1^*}{E_s}\left[1+\frac{E_s^{*2}}{E_t^{*2}}\right]\right] . \tag{129}$$

Here the + is for $A<0$ and the − for $A>0$, and I used the symmetry properties of f_1 and E to relate the terms in $M_L^{(-1)}$ and $M_L^{(+1)}$. Since $\mathrm{Re}E_s > 0$ and $\mathrm{Re}f_1 < 0$ we get for both $A<0$ and $A>0$ the phase matching the phase of M_s. Thus symmetric solutions are allowed. Note however, that in the case of $A>0$, the two quadrupoles near the tip cancel each other. In fact, as the separation goes to zero (i.e., a single wire) the contributions vanish, and the solution will be unstable. For a single perturbation, then, we see that negative perturbations have symmetric solutions, while positive perturbations do not. Let us turn now to this more interesting $A>0$ case.

3. Asymmetry scaling

Consider a τ with one quadrupole to one side of the tip. Say it is on the side so $M_L^{(-1)} \neq 0$, so that $M_L^{(+1)} = 0$. For the perturbation close to the tip, and the asymmetry of the finger small, $\arg(f_1)$ is small. Similarly, for small asymmetry $\arg(M_S)$ is close to $\pi/4$. Therefore, for an $A>0$ quadrupole, the $\pi/2$ phase shift in $M_L^{(-1)}$ has to come from the $(1/E_s(1+E_s^2/E_t^2)$ term. To evaluate the WKBJ integrals analytically, I make the approximation that the constant τ contribution to the integrals can be neglected, thus setting τ equal to 1. For the integral from the tip to $-1/p_2$ this is a fine approximation, but for the leg from the tip to p_s, we will find that it breaks down. Still, if the integral is done numerically with the proper form of τ, it is found that setting $\tau = 1$ is not too bad an approximation. Setting $\tau \cong 1$, gives the appropriate scaling, and a good picture of what is going on. For $\tau = 1$,

$$\arg\left[1+\frac{E_s^2}{E_t^2}\right] \cong 0 \ , \tag{130}$$

so the resonance condition is

$$\mathrm{Im}\frac{1}{G^{1/2}} \int_{-1/p_2}^{p_s} iL^{1/2} d\zeta' = \frac{\pi}{2} + 2n\pi \ , \tag{131}$$

where n is any positive integer. This countable infinity of eigenvalue solutions correspond to the solutions of Vandenbroeck in the constant-τ case. Other work on stability analysis has shown, however, that there are n unstable tip splitting modes associated with these higher n solutions.[33,34] I do not consider the stability of the solutions in the paper, and simply assume the analogous stability results carry over. Thus I will be concerned only with the $n=0$ mode.

The integral from the tip to $-1/p_2$ is pure real, so we can drop that leg. This gives

$$\mathrm{Im}\frac{1}{G^{1/2}}\int_{\mathrm{tip}}^{p_s} iL^{1/2}d\zeta' = \frac{\pi}{2} \tag{132}$$

or, equivalently in l,θ coordinates,

$$\mathrm{Im}\frac{\pi}{2G^{1/2}}\int_0^{l_s} ie^{i\theta/2}dl' = \frac{\pi}{2} \ . \tag{133}$$

This equation, for θ small and setting $|p_s| \simeq 1$, gives

$$l_0 = G^{1/2} \ , \tag{134}$$

where l_0 is the arclength from the perturbation to the tip. The integral can also be done for small asymmetry and p_1 complex, when the perturbation is fixed in the center of the channel. On the finger,

$$\mathrm{Im}z = \lambda - \nu\frac{2\lambda}{\pi} + a \tag{135}$$

(recall $\zeta = e^{i\nu}$ on the finger). The center of the channel, at $\mathrm{Im}z = 0$, is at

$$\nu_{\mathrm{center}} = \frac{\pi}{2}\left[1+\frac{a}{\lambda}\right] \ . \tag{136}$$

To lowest order, the tip is at

$$\nu_{\mathrm{tip}} = \frac{\pi}{2} - \frac{a}{1-\lambda} \ . \tag{137}$$

Near $\zeta = i$ for small a, $L = -\lambda^2$, so

$$P_s = \mathrm{Im}\frac{1}{G^{1/2}}\int_{\nu_{\mathrm{tip}}}^{\nu_{\mathrm{center}}} -\lambda\, d\zeta' = \frac{\pi}{2} \ , \tag{138}$$

which gives

$$a = G^{1/2}\left[1+\frac{\lambda}{1-\lambda}\frac{2}{\pi}\right]^{-1} \ . \tag{139}$$

Thus the asymmetry parameter also scales with $G^{1/2}$.[35] This all is consistent with the scaling results of ZSLK; calling δ the linear displacement of the wire from the tip, they found $\delta \sim G^{0.45\pm0.02}$ in the simulation and $\sim G^{0.40\pm0.04}$ in the experiment over the commonly observable range of G between 5×10^{-3} and 5×10^{-2}. Note, however, that the approximations are inconsistent: I ignored the structure of τ, but now the result is coming from a neighborhood $\sim G^{1/2}$ near the nonconstant part of τ, while the original expression was derived assuming $\sigma, \sigma A \gg G^{1/2}$.

4. λ scaling and Ω effect

We now look at how λ scales with G. The magnitudes of M_S and M_L involve algebraic terms in λ, G, and the exponential E_s. Again the exponential term will dominate the magnitude. For perturbations close to the tip (θ small) the real part of the argument in the exponent comes from the integral from the tip to the singularity at $1/p_2$. For symmetric fingers, changing variables to $x = i\tan\theta$ gives

$$\int_{-1/p_2}^{\mathrm{tip}} iL^{1/2}d\zeta' = \frac{J_\lambda}{K_{\mathrm{tip}}} \ , \tag{140}$$

where

$$K_{\mathrm{tip}} = \frac{1-\lambda}{\lambda^2} \tag{141}$$

is the curvature at the tip and

$$J_\lambda = \int_0^1 \frac{(1-x)^{3/4}(1+x)^{1/4}}{1-x^2\lambda^2/(1-\lambda)^2}dx \tag{142}$$

is some function of λ. Observe, as in the previous section, I have neglected the contributions of $\tau - 1$ to the integral P_s. However, unlike the last section, since the dominant contributions to the integral are coming from the regions where $\tau \simeq 1$, the end result will be consistent. For $\lambda < 1/2$, J_λ is a slowly varying function of λ, and is nearly constant for small λ. Thus, looking at how λ changes for a fixed perturbation as G varies, using (122), (123), (126), and (140) gives

$$K_{\mathrm{tip}} \sim G^{-1/2} \tag{143}$$

for the symmetric finger. This scaling result has been obtained by Hong and Langer,[25] in their model of bubbles as kinks at the tip. Here the result holds as well for perturbations off-centered from the tip, as in the wires. Numerically, I find this scaling is valid for large asymmetries as well. ZSLK found exponents -0.49 ± 0.02 in the simulation and -0.46 ± 0.02 in the experiment.

For small A and σ, f_1 is close to its unperturbed value, and continuing the approximation of neglecting τ in the WKBJ integral, the lowest-order way A and σ enter into the resonance is through the $\sqrt{A\sigma}$ factor in $M_L^{(-1)}$ and $M_L^{(+1)}$. The perturbation can be characterized by this "strength" $\Omega = A\sigma$. For small G and small Ω,

$$K_{\mathrm{tip1}} - K_{\mathrm{tip2}} \approx \tfrac{1}{2}\ln\frac{\Omega_1}{\Omega_2} \ . \tag{144}$$

Rabaud, *et al.*[36] carried out a set of experiments with three different types of perturbations: a bubble, a wire, and grooves along the length of the channel. They found a relative insensitivity to the particular perturbation used in the selected K_{tip} at given G. This logarithmic dependence on Ω explains the relative insensitivity they found. Their conjecture that the selected tip curvature was independent of the kind of perturbation used seems, however, not to be borne out by this analysis.

5. Universality

The universality in the locally perturbed problem comes from two sources. The first is the nature of the terms being balanced. The term M_s comes from an integral over the boundary of the finger. Thus small localized variations leave it essentially unchanged. It depends on the shape of the finger. On the other hand, M_L is a very localized contribution. Its exact form is not important, except to the extent that the symmetry of the solution will depend on the phase difference between it and M_S. The equation for the shape correction (18) could be

dramatically altered in some localized region, and again the net effect would just result in some contribution M_L. This is the reason the exact form of τ is not important.

The second element which produces the universality is that in balancing the two terms—one local and one global—the dominant contribution for small surface tension and small perturbations comes from the exponential E_s. This exponential is an integral which, over typical parameter spaces Ω and G observed exponentially and in simulations, has its major contributions again coming from the shape of the finger. Further, as we saw in section Sec. IV B 2, the effects of perturbations farther away from the tip fall off exponentially. Thus the contributions to M_L come from only the very closest perturbations to the tip. Together, these effects give the scaling laws observed, and the independence of the exact form of τ and even the exact equations that apply in the local region of the perturbed interface. That is the reason the modeling of the physical perturbations by a varying surface tension was possible.

These arguments allow us to expand the suggestion of universality to other systems as well. Using the BPS derivation of the WKBJ solutions—that they are the marginal modes for a curved interface with surface tension—the phenomenology ought to be observable in other problems where a small parameter on the curvature is a singular perturbation on a growing curved front. What changes is $\theta(l)$. In particular, this should hold for dendrites. This work was all done for two-dimensional systems, though it may hold three-dimensional ones as well.

6. *Limits of Ω and G*

As was pointed out in Sec. III D, the analysis required that $|p_2^{3/2}(p_1+p_2)^{3/2}| \gg G$. This becomes relevant when I consider the $\Omega \to 0$ limit. Observe that $M_s \to 0$ as $p_2 \to 0$, so we can satisfy (122) with (123) and (125) for all Ω, with a solution which has $\lambda < 1/2$. The discrepancy comes from the breakdown of the applicability of (123) for $p_2 \to 0$. A discussion of the numerical techniques needed to treat this regime are given in Tanveer. The $\lambda > 1/2$ selection with quadrupole perturbations can also be studied. The region where these solutions can be obtained numerically is, however, within this range of inapplicability of the analytic techniques. I thus do not consider it in this paper. [The local mismatch (125) still holds, and the modification of (123) is quite straightforward. Our symmetry results remain valid.]

The other limit, as $G \to 0$, is intriguing. There, the universality breaks down and we begin to see the structure of τ. The finger turning point $-1/p_2$ and the pole p_s coalesce. The limit is extremely singular: the selection becomes driven by the intimate structure of the singularities of τ, rather than its more averaged properties on the finger. How can this wild behavior be reconciled with a real system? Note that this is precisely the limit where the approximation of isolatedness of the singularities really is true. The deviation must come from a more basic level, the breakdown of our ability to model the physical system with the variable surface tension. The mathematics remains interesting; a thin veneer of universality holding back, for a while, the many-headed beast lurking below.

B. Numerics

In the numerical analysis, it is not necessary to make the approximation that went into the previous sections deriving the scalings. I compare a numerical simulation of the perturbed problem with a numerical solution of the derived resonance condition, providing a stringent quantitative test of the theory. In the simulation, I can put in any perturbation, in particular, the quadrupole used in the theory. The simulation was done using a conformal mapping technique developed by Bensimon.[37] We follow the time evolution of the function which maps the unit circle onto the finger using a fourth-order Runge-Kutta code for the time stepping, and fast Fourier transforms (FFT) for the derivatives and analytic continuations. Numerical instabilities limit how small G can be, and averaging routines are used to try to control them. 512 points evenly spaced on the unit circle were iterated about 10 000 times until a steady state was reached. Periodic boundary conditions were used. This meant that the finger would be symmetric; for $A > 0$ the perturbation would drift to an asymmetric final state, while for $A < 0$ the perturbation would remain at the tip. Thus what was measured was λ and the asymmetry given by $\delta_y = (2/\pi)\lambda(\nu_0 - \nu_{\rm tip})$ in the final state. These were measured as G, A, and σ were varied. Finite spacing of the points limited how small σ could be; $\sigma \geq 0.03$ for 512 points. On the CRAY XMP, the code took about 10 min for 1000 iterations. Most of the time, about 80%, was spent averaging. 15% of the time was spent doing fast Fourier transforms (FFT's), and the rest of the code used the remaining time.

The selection condition balancing (123) and (125) was solved with a two-dimensional Newton's method of iteration. The analytic continuation $f_1(1/p_s)$ was done with an FFT technique. The integrals E_s and E_t were done with a variable step fourth-order Runge-Kutta code.[38] Six parameters were used: λ, a (δ_y for $a=0$), G, A, σ, and y_w where y_w was the fixed value of y of the wire in the channel. Out of the six, any two could be solved for as a function of the other four. A 0.1% accuracy for the fitted parameters was typically obtained after five iterations. Each iteration took about 1 min on a Sun III computer, with the majority of the time being spent on the integration.

The results show very good agreement between theory and simulation. There are no adjustable parameters in the theory, with the result entailing finding a point in a two-dimensional plane. Figure 6 shows λ as a function of G for different strength negative perturbations, which produce a symmetric state. The solid curves are the theory, and the data points come from the simulation. As pointed out in Sec. V A6, for $a=0$ as in the simulations, (123) is valid only for $|\frac{1}{2}-\lambda| \gg G^{2/3}$. In Figs. 6 and 7 I show with a dashed line the curve $\frac{1}{2}-\lambda = G^{2/3}$. Figure 7 shows λ as a function of G for positive perturba-

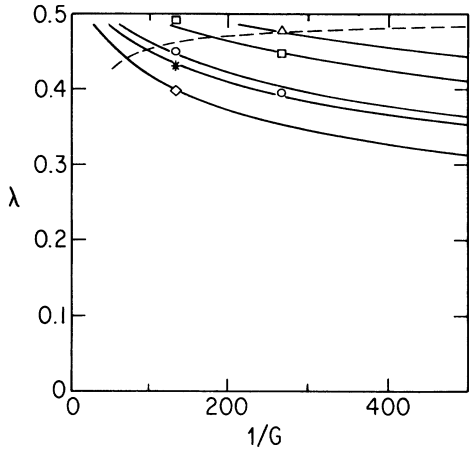

FIG. 6. Finger width λ vs $1/G$ for one $A<0$ quadrupole perturbation. The solid lines are theory, and the data points are from the simulation. Stronger perturbations correspond to smaller λ curves. The dotted line is the line $\frac{1}{2}-\lambda=G^{2/3}$; near and above this line the theory is not valid. ◇, $A=-0.5$, $\sigma=0.03$; *, $A=-0.125$, $\sigma=0.05$; ○, $A=-0.1$, $\sigma=0.03$; □, $A=-0.01$, $\sigma=0.03$; △, $A=-0.001$, $\sigma=0.03$.

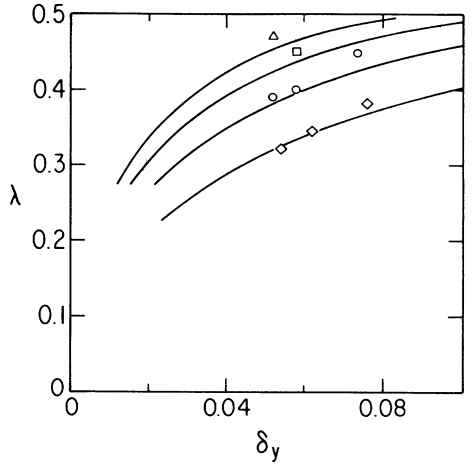

FIG. 8. One $A>0$ quadrupole perturbation. Solid lines are theory, data points are simulation. Stronger perturbations correspond to smaller λ curves. The finger width λ is plotted on the vertical axis, and the asymmetry δ_y is plotted on the horizontal axis. The lines correspond to varying G for a given A, σ. In each case $\sigma=0.03$. ◇, $A=1.0$; ○, $A=0.1$; □, $A=0.01$; △, $A=0.001$.

tions. Figure 8 shows δ_y and λ for different positive perturbations as G is varied. From (134) we see that for small values of δ_y, the lines of constant G in Fig. 8 will be vertical. One more comment on the figures: because the simulation is so expensive—about 1.5 h on the Cray per data point, the number of data points from the simulation was quite limited. That is the reason for the sparseness of the data in the figures.

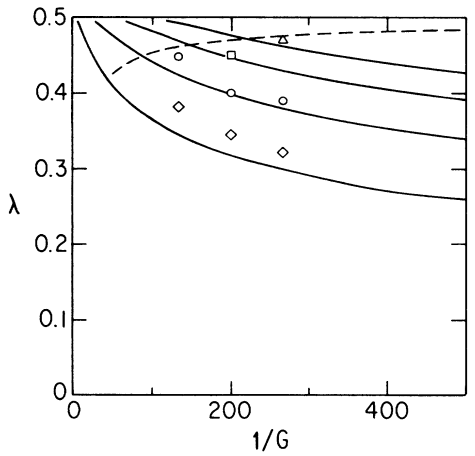

FIG. 7. Finger width λ vs $1/G$ for one $A>0$ quadrupole perturbation. The solid lines are theory, and the data points are from the simulation. Stronger perturbations correspond to smaller λ curves. The asymmetry of these fingers is not shown in this plot. In each case $\sigma=0.03$. The dotted line is the line $\frac{1}{2}-\lambda=G^{2/3}$; near and above this line the theory is not valid. ◇, $A=1.0$; ○, $A=0.1$; □, $A=0.01$, △, $A=0.001$.

1. *Comparison of theory and simulation*

For λ near $\frac{1}{2}$ we run into the range where the analytic theory breaks down. Unfortunately, most of the data I could obtain fall outside the range where Eq. (123) is valid [the solid lines for the theory were calculated with (123)]. Noise in the simulation limited how small G could be. At the smallest values of G, λ became unsteady giving a larger uncertainty in λ at the smallest values of G. The uncertainty for δ_y comes from the finite grid spacing of the points, and is $\sim\lambda/512$ with the number 512 coming from the number of points used in the simulation. The size of these contributions to the uncertainty is smaller than the size of the points in the figures. There is an additional source of error in the simulation data, as to when a steady state is reached. The criterion used was that there be no change in λ for at least one finger width growth down the channel. This criterion is not always sufficient, however, and there are unknown uncertainties for each simulation data point associated with possibly not having reached a steady state.

In all cases, as mentioned in Sec. IV A the assumption of isolatedness of the singularities, that $\sigma \ll G^{1/2}$ was not at all true. In addition, the theory is done with n in (131) large, while in the end I took the lowest mode. The size of these last two effects is not known. The astonishing thing is how well the theory and simulation actually agree; again, there are no free parameters to do the fitting. The best region for quantitative comparison is for λ away from $\frac{1}{2}$ and G small. For the data there, the deviations are less than 5% in λ and in δ_y between theory and

simulation. Putting it another way, for the data below the $\frac{1}{2}-\lambda=G^{2/3}$ curve, we would only have to multiply one of the mismatch functions by a constant between 0.8 and 1.5 in order to superimpose the theory curve on the simulation data.

C. Connection to Experiments

There are a number of features of the theory that ought to be observable experimentally. Of course, the form of the experimental perturbation is not known, but to the extent to which that does not matter, the theory will have things to say. The essential source of the universality, as discussed in Sec. VI A 5, is how the WKBJ integral drives the selection; there, it is the sign and strength of the perturbation, and where it is on the interface that matters. Physically, the differential equation can be thought of (117) as representing some response of some stiff object to a displacement. We have basically an oscillator equation, with complex coefficients varying slowly compared to the length scale $G^{1/2}$. That perturbations far from the tip have a smaller effect makes sense physically, as much of the growth is happening at the tip. What is less obvious is the phase associated with the magnitude of this effect; a perturbation moving along the interface would alternately constructively and destructively interfere with the scattering from the finger singularity. By considering a stiff object, with a length scale of bending of $G^{1/2}$, the origin of this phase can be seen: pushing down on a neighboring maximum and minimum tend to cancel each other.

1. Two-wire interference experiment

One way to probe this phase effect experimentally is to set up an experiment with two wires on one side, looking at the variation in λ as the spacing is varied at a given G, and compare it to a single wire. For $G^{1/2}$ large compared to the wire spacing, the two wires look like one stronger wire so λ for the two wires is smaller than for the single wire. As $G^{1/2}$ becomes comparable to the separation, though, there is some phase difference between the two wires, so that eventually they destructively interfere, and λ is larger than for the single wire. As $G^{1/2}$ is further reduced, they begin to constructively interfere again. Thus the width oscillates about the single wire values as the wires alternately constructively and destructively interfere. As the wire separation is changed, this crossover to the oscillating region changes. We are only concerned with the phase difference between the wires. This leads to the restriction of the case of both wires being on the same side of the tip. At the same time, the phenomena will be present for asymmetric fingers as well. For separation of the wires d in the channel of width w, the peaks and valleys of the λ oscillations will occur at integer values n:

$$\frac{d/w}{G^{1/2}}=n \quad \begin{cases}\text{peak}, & n \text{ odd} \\ \text{valley}, & n \text{ even} .\end{cases} \tag{145}$$

The relation is valid in the limit of

$$\sigma \ll d/w \ll \lambda . \tag{146}$$

The number of oscillations that could be seen can be estimated as follows: take $\lambda \approx \frac{1}{2}$; the wire separation can be about $\frac{1}{10}$ of λ, or about $\frac{1}{20}$ of the channel width. Values of $G^{1/2}$ of $\frac{1}{80}$ can be obtained (ZSLK). That gives $n=4$. This of course assumes the wires have the same strength. To get cancellation, they would have to be quite close in magnitude; they should be observable if they do not differ by more than a factor of 2. Using (126) and (140) this then puts a limit on θ of the second wire:

$$(\pi/4)G^{-1/2}K_{\text{tip}}^{-1}\theta_{\text{wire}}^2 \lesssim 1 .$$

The problem is that for a wire separation of $\frac{1}{20}$ the channel width, for $k_{\text{tip}} \approx \pi$ and $G^{-1/2} \approx 80$ the effect of the second wire is reduced by e^{-2}. Thus it will be extremely difficult to see anything past $n=2$. One way to compensate for this effect is to replace the wire farther away from the tip with a stronger Ω wire. One would measure an effective Ω for a wire by performing experiments with that single wire in the channel, and then match two wires of different strengths. The procedure seems difficult, but it also becomes a test of the falloff in the real part of the WKBJ integral.

From the arguments on universality given in Sec. V A 5, this interference effect is a general one for growing curved fronts where surface tension is the singular perturbation giving selection. Thus this relation should be valid for two-dimensional dendrites as well.[39] It may also be valid for free three-dimensional dendrites.

2. Phase difference from tip experiment

The prediction that the wires lie a phase $\pi/2$ from the tip should be studied. A direct quantitative test of (134) can be performed. The problem is that there is no regime where it actually is valid. The agreement with (134) will depend on how much of the $\pi/2$ phase is coming from the WKBJ integral with $\tau=1$; that is, we want $\sigma \ll 1$ and the wire close to the tip, but not too close. Qualitative agreement may be the best that can be hoped for.

The requirement that the perturbation be close to the tip can be loosened if the phase from f_1 is included, and any phase from the asymmetry of the finger. These are calculable constants which can be subtracted out, though they make the expression for l_0 messier.

A test that might be less sensitive to the phase contribution from $\tau-1$ might be performed as follows. Place a single wire in the channel a distance d from the center. Find the value of G where the asymmetry parameter goes to zero; call is G_0. This tells us how far away from a symmetric finger the wire would optimally be. Now explore the phase structure by putting in four symmetric wires in the channel: two at $\pm d$ and two at $\pm D$, where $D>d$. As D is made larger, there will be oscillations in λ, about the two $\pm d$ wire curve, wich die out as D becomes large compared to d. At fixed G_0, there should be a maximum in λ when $D=3d$. Let us see what happens if the contribution to the phase of the local structure of the perturbation can be ignored, as was done in Sec. V A 3. The contribution to the phase by the wire and the other position dependent terms will not be zero. The best

place to minimize the other contributions will be a balance between the desire for large d to minimize σ effects, and small d to minimize θ and f_1 effects.

3. *Characterization of experimental perturbation strengths*

Another quantitative test of the theory may be possible if the "strength" Ω of the wire remains relatively constant as we vary G or the lateral placement of the wire in the channel. Then, given a measurement of Ω and the asymmetry at one value of G and placement of the wire in the channel, it would be possible to predict the values of λ for other values where Ω is invariant. Note that we most likely do not have predictability of the asymmetry: the details of the perturbation enter in quantitatively there. All this depends on the three dimensional flow around the wire; it is an experimental question whether the effective Ω remains constant enough to give predictability in any region.[40]

VI. CONCLUSION

I have developed a theory for localized perturbations in the Saffman-Taylor problem. The source of the universality in the locally perturbed problem has been discussed, giving some explanation of why the physically complicated experimental perturbations can be modeled by locally varying surface tension. The results are in agreement with the phenomenology reported by ZSLK for perturbed fingers. I have obtained very good quantitative agreement between theory and simulation, with no adjustable parameters to fit. Finally, I have outlined experiments to observe new effects predicted by the theory. An important physical effect is the presence of a phase associated with the magnitude for perturbations on the interface. This effect is a general one for growing curved fronts with a surface energy term. A quantitative relation illuminating this effect has been given; this prediction should be observable experimentally.

ACKNOWLEDGMENTS

I would like to thank Leo Kadanoff for his generous encouragement and support. I also thank him for his many thoughtful suggestions in making this paper clearer and more readable. I have benefited much from discussions with Albert Libchaber. Suleh Tanveer has answered numerous questions on his method, and I am grateful that he left the problem alone while I worked through it. Pierre Pelce provided helpful discussions in the early stages. I thank David Bensimon for the use of his program. This work was supported by the National Science Foundation under grant No. NSF DMR 8316626. This work was partially supported by the National Center for Supercomputing Applications and utilized the CRAY X-MP System at National Center for Supercomputing Applications (NCSA) at the University of Illinois at Urbana–Champaign. This work was presented as a thesis to the Department of Physics, the University of Chicago, in partial fulfillment of the requirements for the Ph.D. degree.

[1]J. S. Langer, Rev. Mod. Phys. **52**, 1 (1980).
[2]Y.Sawada, A. Dougherty, and J. P. Gollub, Phys. Rev. Lett. **56**, 1260 (1986).
[3]D. Grier, E. Ben-Jacob, R. Clarke, and L. M. Sander, Phys. Rev. Lett. **56**, 1264 (1986).
[4]T. Halsey, Phys. Rev. A **36**, 3512 (1987).
[5]T. A. Witten and L. M. Sander, Phys. Rev. B **27**, 5696 (1983).
[6]H. S. Hele-Shaw, Nature **58**, 34 (1898).
[7]J. S. Langer, *Lectures in the Theory of Pattern Formation*, 1986 Les Houches Lectures (North-Holland, Amsterdam, in press).
[8]J. Nittman, G. Daccord, and H. E. Stanley, Nature **314**, 141 (1985).
[9]D. Bensimon, L. P. Kadanoff, S. Liang, B. Shraiman, and C. Tang, Rev. Mod. Phys. **58**, 977 (1986).
[10]P. G. Saffman, Q. J. Mech. Appl. Math **12**, 146 (1959); D. Howison, T. R. Ockendon, and A. A. Lacey, Q. J. Mech. Appl. Math. **38**, 343 (1985); B. Shraiman and D. Bensimon, Phys. Rev. A **30**, 2840 (1984); D. Bensimon and P. Pelce, Phys. Rev. A **33**, 4477 (1986).
[11]G. P. Ivantsov, Dokl. Akad. Nauk. SSSR **58**, 567 (1947).
[12]D. Kessler and H. Levine (unpublished).
[13]P. Pelce, *The Dynamics of Curved Fronts* (McGraw-Hill, New York, in press).
[14]G. I. Taylor and P. G. Saffman, Q. J. Mech. Appl. Math. **12**, 265 (1959).
[15]P. G. Saffman and G. I. Taylor, Proc. R. Soc. London, Ser. A **245**, 312 (1958).
[16]J. W. McLean and P. G. Saffman, J. Fluid Mech. **102**, 445 (1981).
[17]B. Shraiman, Phys. Rev. Lett. **56**, 2028 (1986).
[18]D. C. Hong and J. S. Langer, Phys. Rev. Lett. **56**, 2032 (1986).
[19]R. Combescot, T. Dombre, V. Hakim, Y. Pomeau, and A. Pumir, Phys. Rev. Lett. **56**, 2036 (1986).
[20]L. Pokrovskii and I. M. Khalatnikov, Zh. Eksp. Teor. Fiz. **40**, 1713 (1961) [Sov. Phys.—JETP **13**, 1207 (1961)].
[21]M. Kruskal and H. Segur (unpublished).
[22]Y. Couder, N. Gerard, and M. Rabaud, Phys. Rev. A **34**, 5175 (1986).
[23]G. Zocchi, B. E. Shaw, A. Libchaber, and L. P. Kadanoff, Phys. Rev. A **36**, 1894 (1987).
[24]J. R. Grace and D. Harrison, Chem. Eng. Sci. **22**, 1337 (1967). They found narrowed solutions in two and three dimensions when the bubble surrounded a rod that was placed in the channel.
[25]D. C. Hong and J. S. Langer, Phys. Rev. A **36**, 2325 (1987).
[26]D. C. Hong, Phys. Rev. A **37**, 2724 (1989).
[27]S. Tanveer, Phys. Fluids **30**, 1589 (1987).
[28]J. S. Langer, Phys. Rev. A **33**, 435 (1986).
[29]C. Bender and S. Orszag, *Advanced Mathematical Methods for Scientists and Engineers* (McGraw-Hill, New York, 1978).
[30]F. W. J. Oliver, *Asymptotics and Special Functions* (Academic, New York, 1974).
[31]W. Wasow, *Linear Turning Point Theory* (Springer-Verlag, New York, 1985).
[32]D. Bensimon, P. Pelce, and B. Shraiman, J. Phys. (Paris) B **47**, 2081 (1987).
[33]D. A. Kessler and H. Levine, Phys. Rev. Lett. **57**, 3069 (1986).
[34]S. Tanveer, Phys. Fluids **30**, 2318 (1987).

[35]After completing this paper I received a copy of unpublished work from D. C. Hong where he obtains a similar result for the asymmetry scaling.

[36]M. Rabaud, Y. Couder, and N. Gerard, Phys. Rev. A **37**, 935 (1988).

[37]D. Bensimon, Phys. Rev. A **33**, 1302 (1986).

[38]W. H. Press, B. P. Flanney, S. A. Teukolsky, and W. T. Vetterling, *Numerical Recipes* (Cambridge University Press, Cambridge, MA, 1986).

[39]J. Bechhoefer, H. Guido, and A. Libchaber, C. R. Acad. Sci. Paris **306**, 619 (1988).

[40]I have recently begun a set of experiments to test the predictions in this paper. Preliminary results show qualitative agreement with Eq. (139), though there is a quantitative discrepancy. The finite contact angle appears to matter, and as was noted at the end of Sec. V A 3 the neighborhood of the perturbation was contributing to the phase. This discrepancy may make the interference effect of Sec. V C 3 unobservable. On the other hand, the characterization of weak perturbations in selecting λ by a single real number Ω seems to work well in the experiments.